

High-precision abundances of elements in solar twin stars [★]

Trends with stellar age and elemental condensation temperature

P. E. Nissen¹

Stellar Astrophysics Centre, Department of Physics and Astronomy, Aarhus University, Ny Munkegade 120, DK-8000 Aarhus C, Denmark. e-mail: pen@phys.au.dk.

Received 7 April 2015 / Accepted

ABSTRACT

Context. High-precision determinations of abundances of elements in the atmospheres of the Sun and solar twin stars indicate that the Sun has an unusual low ratio between refractory and volatile elements. This has led to the suggestion that the relation between abundance ratios, $[X/Fe]$, and elemental condensation temperature, T_C , can be used as a signature of the existence of terrestrial planets around a star.

Aims. HARPS spectra with $S/N \gtrsim 600$ for 21 solar twin stars in the solar neighborhood and the Sun (observed via reflected light from asteroids) are used to determine very precise ($\sigma \sim 0.01$ dex) differential abundances of elements in order to see how well $[X/Fe]$ is correlated with T_C and other parameters such as stellar age.

Methods. Abundances of C, O, Na, Mg, Al, Si, S, Ca, Ti, Cr, Fe, Ni, Zn, and Y are derived from equivalent widths of weak and medium-strong spectral lines using MARCS model atmospheres with parameters determined from the excitation and ionization balance of Fe lines. Non-LTE effects are considered and taken into account for some of the elements. In addition, precise ($\sigma \lesssim 0.8$ Gyr) stellar ages are obtained by interpolating between Yonsei-Yale isochrones in the $\log g$ - T_{eff} diagram.

Results. It is confirmed that the ratio between refractory and volatile elements is lower in the Sun than in most of the solar twins (only one star has the same $[X/Fe]$ - T_C distribution as the Sun), but for many stars, the relation between $[X/Fe]$ and T_C is not well defined. For several elements there is an astonishingly tight correlation between $[X/Fe]$ and stellar age with amplitudes up to ~ 0.20 dex over an age interval of eight Gyr in contrast to the lack of correlation between $[Fe/H]$ and age. While $[Mg/Fe]$ increases with age, the s -process element yttrium shows the opposite behavior meaning that $[Y/Mg]$ can be used as a sensitive chronometer for Galactic evolution. $[Na/Fe]$ and $[Ni/Fe]$ are not well correlated with stellar age, but define a tight Ni-Na relation similar to that previously found for more metal-poor stars albeit with a smaller amplitude. Furthermore, the C/O ratio evolves very little with time, although $[C/Fe]$ and $[O/Fe]$ change by ~ 0.15 dex.

Conclusions. The dependence of $[X/Fe]$ on stellar age and the $[Ni/Fe]$ - $[Na/Fe]$ variations complicate the use of the $[X/Fe]$ - T_C relation as a possible signature for the existence of terrestrial planets around stars. The age trends for the various abundance ratios provide new constraints on supernovae yields and Galactic chemical evolution, and the slow evolution of C/O for solar metallicity stars is of interest for discussions of the composition of exoplanets.

Key words. Stars: abundances – Stars: fundamental parameters – Stars: solar-type – (Stars:) planetary systems – Galaxy: disk – Galaxy: evolution

1. Introduction

In an important paper based on very precise determinations of abundances in the Sun and 11 solar twin stars, Meléndez et al. (2009) found that the Sun has a lower refractory to volatile element ratio than most of the solar twins. They suggest that this may be explained by the sequestration of refractory elements in terrestrial planets and that the slope of abundances relative to iron, $[X/Fe]$ ¹, as a function of elemental condensation temperature, T_C , in a solar-composition gas (Lodders 2003) can be used as a signature of the existence of terrestrial planets around a star. This idea was supported by Ramírez et al. (2009), who in a study of abundances of 64 solar-type stars find significant variations of

the $[X/Fe]$ - T_C slope with only about 15% of the stars having a slope similar to that of the Sun.

The works of Meléndez et al. (2009) and Ramírez et al. (2009) have triggered several papers investigating relations between $[X/Fe]$ - T_C slopes and existence of planets around stars (Gonzalez et al. 2010; González Hernández et al. 2010, 2013; Schuler et al. 2011; Adibekyan et al. 2014; Maldonado et al. 2015). The results obtained are not so conclusive, partly because the stars included span larger ranges in T_{eff} , $\log g$, and $[Fe/H]$ than the solar twins in Meléndez et al. (2009) making the abundance ratios less precise and introducing a dependence of the derived $[X/Fe]$ - T_C slopes on possible corrections for Galactic evolution effects. Thus, González Hernández et al. (2013) obtain both positive and negative slopes for ten stars with detected super-Earth planets, and Adibekyan et al. (2014) find evidence that the slope depends on stellar age. Furthermore, Schuler et al. (2011) show that the $[X/Fe]$ - T_C slope depends critically on whether one consider refractory elements only ($T_C > 900$ K) or include also volatile elements with $T_C < 900$ K.

[★] Based on data products from observations made with ESO Telescopes at the La Silla Paranal Observatory under programs given in Table 1. Tables 2 and 3 are available in electronic form at <http://www.aanda.org>.

¹ For two elements, X and Y, with number densities N_X and N_Y , $[X/Y] \equiv \log(N_X/N_Y)_{\text{star}} - \log(N_X/N_Y)_{\text{Sun}}$.

Sequestration in terrestrial planets is not the only possible explanation of the low abundances of refractory elements in the Sun. Önehag et al. (2014) found that the $[X/Fe]-T_C$ trend for solar-type stars belonging to the open cluster M 67 agrees with the trend for the Sun and suggest that the gas of the proto-cluster was depleted in refractory elements by formation and cleansing of dust before the stars formed. According to this, the Sun may have formed in a dense stellar environment contrary to most of the solar twins. Similar scenarios are discussed by Gaidos (2015), who suggests that $[X/Fe]-T_C$ correlations can be explained by dust-gas segregation in circumstellar disks rather than formation of terrestrial planets.

Additional information on the connection between abundance ratios in stars and the occurrence of planets may be obtained from studies of wide binaries for which the two components have similar T_{eff} and $\log g$ values. Dust-gas segregation before planet formation is likely to affect the chemical composition of the components in the same way. In the case of 16 Cyg A/B, for which the secondary component has a detected planet of at least 1.5 Jupiter mass (M_J), there is a difference $[Fe/H](A-B) \approx 0.04$ dex (Ramírez et al. 2011) and a difference in the $[X/Fe]-T_C$ slope for refractory elements (Tucci Maia et al. 2014), which may be explained by accretion of elements in the rocky core of the giant planet around 16 Cyg B. Furthermore, the two components of XO-2, which are hosts of different planets, have an abundance difference of ~ 0.05 dex for refractory elements (Teske et al. 2015; Damasso et al. 2015). On the other hand, Liu et al. (2014) did not detect any abundance differences between the two components of HAT-P-1, for which the secondary has a $0.5M_J$ planet.

Recent precise determinations of abundances in four solar twin stars: HD101364 (Meléndez et al. 2012), HIP 102152 (HD197027) (Monroe et al. 2013), 18 Sco (HD 146233) (Meléndez et al. 2014a), and HD218544 (Meléndez et al. 2014b) show that the first three mentioned stars have a similar depletion of refractory elements as the Sun, whereas 18 Sco has a $[X/Fe]-T_C$ slope for elements from carbon to zinc similar to the majority of solar twin stars. Neutron capture elements in 18 Sco are, however, significantly more abundant than lighter elements with the same condensation temperature, and in HIP 102152 several elements (N, Na, Co, and Ni), have abundance ratios with respect to Fe that clearly fall below the $[X/Fe]-T_C$ trend for the other elements. These anomalies suggest that the $[X/Fe]-T_C$ relation is not so well defined as assumed in some of the works cited above, but that star-to-star variations in abundance ratios related to e.g. incomplete mixing of nucleosynthesis products or chemical evolution play a role.

In order to make further studies of $[X/Fe]-T_C$ relations, I have derived very precise abundance ratios ($\sigma[X/Fe] \sim 0.01$ dex) for a sample of 21 solar twin stars for which high-resolution HARPS spectra with signal-to-noise (S/N) ratios ranging from 600 to more than 2000 are available. For the Sun a HARPS spectrum with $S/N \approx 1200$ of reflected sunlight from Vesta is used. The sample is not well-suited for studying relations between abundance ratios and occurrence of planets, because only three of the stars are known to be hosts of planets. On the other hand, it is possible to study how well abundance ratios are correlated with T_C and to see if $[X/Fe]$ depends on other parameters such as stellar age.

2. Observational data

Based on the precise effective temperatures, surface gravities and metallicities derived by Sousa et al. (2008) from HARPS spec-

tra of FGK stars, a sample of solar twins was selected to have parameters that agree with those of the Sun within ± 100 K in T_{eff} , ± 0.15 dex in $\log g$, and ± 0.10 dex in $[Fe/H]$. Listed in Table 1, 21 of these stars have HARPS spectra with $S/N \geq 600$ after combination of spectra available in the ESO Science Archive.

The HARPS spectra have a resolution of $R \approx 115\,000$ (Mayor et al. 2003). Individual spectra for a given star were combined after correction for Doppler shifts and then normalized with the IRAF `continuum` task using cubic splines with a scale length of ~ 100 Å in the blue spectral region (3800 - 5300 Å) and ~ 15 Å in the red region (5350 - 6900 Å), for which the archive spectra are more irregular. The S/N values given in Table 1 were estimated from the rms variation of the flux in continuum regions for the 4700 - 6900 Å spectral region, which contains the spectral lines applied in this study. By including spectra obtained from 2011 to 2013 (programs 183.C-0972 and 188.C-0265), the S/N is in most cases significantly higher than that of the HARPS spectra applied in previous studies of solar twin stars (e.g., González Hernández et al. 2010, 2013). For the stars in Table 1, the S/N ranges from 600 to 2400 with a median value of 1000.

The IRAF `splot` task was used to measure equivalent widths (EWs) of spectral lines by Gaussian fitting relative to pseudo-continuum regions lying within 3 Å from the line measured. These regions do not necessarily represent the true continuum, but care was taken to use the same continuum windows in all stars, so that differences in EW between stars are precisely measured given that the same instrument and resolution were applied for obtaining spectra. In this way differential abundances may be obtained with a precision better than 0.01 dex as shown by Bedell et al. (2014).

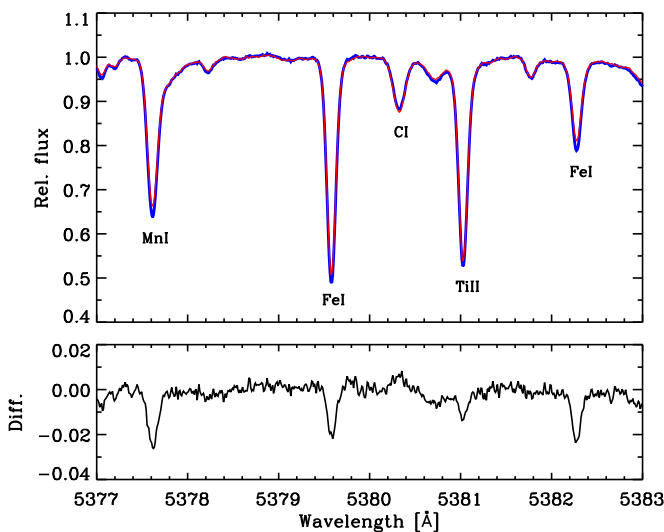
In order to achieve high-precision abundances relative to the Sun, it is very important that a solar flux spectrum is obtained with the same spectrograph as applied for the solar twin stars (Bedell et al. 2014). As listed in Table 1, several such HARPS spectra are available based on reflected light from asteroids and the Jupiter moon Ganymede. As the prime reference spectrum for the Sun, the Vesta spectrum with $S/N \approx 1200$ is adopted, but it is noted that the Ceres and Ganymede spectra agree very well with that of Vesta. Equivalent widths measured in the Vesta spectrum and the combined spectrum of Ceres and Ganymede ($S/N \approx 700$) have an rms difference of 0.35 mÅ only.

To illustrate the high quality of the spectra applied and the differential way of measuring EWs, Fig. 1 shows a comparison of the Vesta spectrum with that of HD 27063, which turns out to have a very similar effective temperature ($T_{\text{eff}} = 5779$ K) and surface gravity ($\log g = 4.47$) as the Sun. As seen from the difference between the spectra in the lower panel of Fig. 1, lines corresponding to refractory elements are somewhat stronger in the spectrum of HD 27063 than in the solar spectrum, whereas the line of the volatile element carbon at 5380.3 Å is a bit stronger in the solar spectrum. HD 27063 turns out to be a star with a high refractory to volatile ratio compared to the Sun; i.e. $[Fe/H] = 0.064$ and $[C/H] = -0.018$.

Oxygen is an important volatile element in addition to carbon. Unfortunately, the HARPS spectra do not cover the O I triplet at 7774 Å. Instead, the forbidden oxygen line at 6300.3 Å was used to derive $[O/H]$. For six stars telluric O₂ lines happen to disturb the [O I] line in some of the spectra available. Such spectra were excluded before making a combination of spectra to be used in the [O I] region. This decreased the S/N of the [O I] spectra somewhat, but in all cases it is around or above 500.

Table 1. ESO/HARPS observing programs and S/N of combined spectra.

Star	ESO/HARPS program numbers	S/N
HD 2071	072.C-0488, 183.C-0972, 188.C-0265	1050
HD 8406	072.C-0488, 183.C-0972	700
HD 20782	072.C-0488, 183.C-0972	1250
HD 27063	072.C-0488	850
HD 28471	072.C-0488, 183.C-0972	700
HD 38277	072.C-0488, 183.C-0972	900
HD 45184	072.C-0488, 183.C-0972	2400
HD 45289	072.C-0488, 183.C-0972, 188.C-0265	1250
HD 71334	072.C-0488, 183.C-0972, 188.C-0265	900
HD 78429	072.C-0488	1200
HD 88084	072.C-0488, 183.C-0972	800
HD 92719	072.C-0488, 183.C-0972	1150
HD 96116	072.C-0488, 183.C-0972, 188.C-0265	600
HD 96423	072.C-0488, 183.C-0972, 188.C-0265	1200
HD 134664	072.C-0488	850
HD 146233	072.C-0488	850
HD 183658	072.C-0488, 183.C-0972, 188.C-0265	1000
HD 208704	072.C-0488, 183.C-0972, 188.C-0265	1100
HD 210918	072.C-0488	1300
HD 220507	072.C-0488, 183.C-0972, 188.C-0265	1100
HD 222582	072.C-0488, 183.C-0972	1000
Vesta	088.C-0323	1200
Ceres	082.C-0357, 060.A-9036, 060.A-9700	500
Ganymede	060.A-9036, 060.A-9700	450


Fig. 1. The solar flux HARPS spectrum around the C I line at 5380 Å obtained via reflected light from Vesta (thin, red line) in comparison with the HARPS spectrum of HD 27063 (thick, blue line). The lower panel shows the difference (HD 27063 – Sun) between the two spectra.

3. Model atmosphere analysis

The Uppsala EQWIDTH program, which is based on the assumption of local thermodynamic equilibrium (LTE), was used to calculate equivalent widths as a function of element abundance for plane parallel (1D) MARCS model atmospheres (Gustafsson et al. 2008) representing the stars. Interpolation to the observed EWs then yields the LTE abundances for the various elements.

3.1. Spectral lines

The spectral lines used are listed in Table 2. As seen, they fall in the spectral region 4700 – 6900 Å, where the S/N of HARPS spectra is higher and line blending less severe than in the blue region. Strong lines, such as the NaD lines and the Mgb triplet, and lines significantly blended by stellar or telluric lines were avoided except for the [O I] λ 6300.3 line, which is blended by a Ni I line. For C, Na, Mg, and Al two lines are available for each element. Heavier elements have at least three lines and for Ti, Cr, and Fe both neutral and ionized lines are available. In the case of Fe, only lines having $EW_{\text{Sun}} < 70 \text{ m}\text{\AA}$ were included. This results in a list of 47 Fe I lines with excitation potentials, χ_{exc} , ranging from 0.9 to 5.1 eV and nine Fe II lines, which are used to determine effective temperatures and surface gravities of the stars as described in Sect. 3.2.

As the analysis is made differentially to the Sun line by line, the gf -values of the spectral lines cancel out. Doppler broadening due to microturbulence is specified by a depth-independent parameter, ξ_{turb} . Collisional broadening of Ca I, Ti I, Cr I, Fe I, Fe II, and Ni I lines caused by neutral hydrogen and helium atoms is based on quantum mechanical calculations (Anstee & O’Mara 1995; Barklem & O’Mara 1998; Barklem et al. 2000; Barklem & Aspelund-Johansson 2005). For the remaining lines, the Unsöld (1955) approximation with an enhancement factor of two was applied. If instead an enhancement factor of one is adopted, the differential abundances are not changed significantly due to the fact that the damping wings of the lines only contribute a small fraction of the equivalent width.

The derivation of oxygen abundances impose a particular problem, because the [O I] λ 6300.3 line is blended by a Ni I line with nearly the same wavelength (Allende-Prieto et al. 2001). Based on the MARCS solar model, $\log gf = -2.11$ (Johansson et al. 2003), and a solar nickel abundance of $A(\text{Ni})_{\odot} = 6.15$ (as determined from 17 weak Ni I lines listed in Scott et al. 2009), the equivalent width of the Ni I line is calculated to be 1.7 mÅ. After subtracting this value from the measured EW of the [O I] – Ni I blend (5.3 mÅ), one gets $EW([\text{O I}])_{\odot} = 3.6 \text{ m}\text{\AA}$. For the stars, the measured EWs of the [O I] – Ni I blend were corrected in the same way by subtracting the EW of the Ni I line as calculated for the model atmosphere of the star and the [Ni/H] value derived.

3.2. Stellar parameters

Adopting solar parameters, $T_{\text{eff}} = 5777 \text{ K}$, $\log g = 4.438$, and $\xi_{\text{turb}} = 1.0 \text{ km s}^{-1}$, the corresponding parameters of the stars were determined by requesting that [Fe/H] has no systematic dependence on χ_{exc} and EW of the lines and that the mean [Fe/H] values derived from Fe I and Fe II lines, respectively, are equal. The slope of [Fe/H] as a function of excitation potential is sensitive to the effective temperature and the slope of [Fe/H] versus EW depends on the microturbulence. The difference of [Fe/H] derived from Fe I and Fe II lines depends on the surface gravity via its effect on the electron pressure in the stellar atmospheres, but it is also affected by the iron and α -element abundances, because these elements are important electron donors. Therefore, it is necessary to make a number of iterations using MARCS models with different parameters T_{eff} , $\log g$, [Fe/H], and $[\alpha/\text{Fe}]$ to ensure that the excitation and ionization balance of Fe lines are fulfilled. These models are obtained from two sets of MARCS models: the standard set with $[\alpha/\text{Fe}] = 0$ at [Fe/H] ≥ 0 and $[\alpha/\text{Fe}]$ rising linearly to $[\alpha/\text{Fe}] = 0.4$ when [Fe/H] decreases from 0.0 to -1.0 , and the α -enhanced set with $[\alpha/\text{Fe}] = 0.4$ at all metallicities.

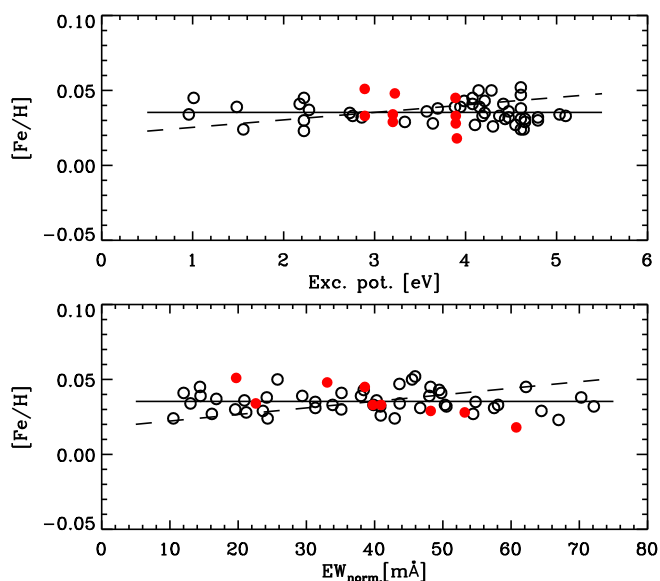


Fig. 2. [Fe/H] derived from lines in the spectrum of HD 183658 as a function of excitation potential (upper panel) and “normalized” equivalent width: $EW_{\text{norm.}} = EW \cdot 6000.0/\lambda$ [Å] (lower panel). Open circles refer to Fe I lines and filled (red) circles to Fe II lines. The full drawn lines show linear fits to the Fe I data for the derived parameters of the star. The dashed lines show changes in the slopes if T_{eff} is decreased by 30 K (upper panel) and the microturbulence is decreased by 0.1 km s^{-1} (lower panel).

Hence, it is possible to interpolate to a MARCS model with the $[\alpha/\text{Fe}]$ value² of a star. This is of some importance for three α -enhanced solar twins in this paper with $[\alpha/\text{Fe}] \approx 0.08$. If models with $[\alpha/\text{Fe}] = 0.0$ were adopted for these stars, the derived effective temperature and gravity would change by $\Delta T_{\text{eff}} \approx -8 \text{ K}$ and $\Delta \log g \approx +0.025 \text{ dex}$, whereas the effect on [Fe/H] is only -0.003 dex .

As a typical example, Fig. 2 shows [Fe/H] as a function of χ_{exc} and EW obtained with the final model of HD 183658 (T_{eff} , $\log g$, [Fe/H], $[\alpha/\text{Fe}]$) = (5809 K, 4.402, +0.035, 0.007). The rms scatter of [Fe/H] is 0.007 dex for Fe I lines and 0.011 dex for Fe II lines. Based on the 1-sigma errors of the slopes of [Fe/H] versus χ_{exc} and EW and the errors of the average Fe abundances derived from Fe I and Fe II lines, respectively, the error analysis method described by Epstein et al. (2010) and Bensby et al. (2014) has been used to derive the errors of T_{eff} , $\log g$, [Fe/H], and ξ_{turb} . The estimated errors are nearly the same for all stars, i.e., $\sigma(T_{\text{eff}}) = 6 \text{ K}$, $\sigma(\log g) = 0.012 \text{ dex}$, $\sigma([\text{Fe}/\text{H}]) = 0.006 \text{ dex}$, and $\sigma(\xi_{\text{turb}}) = 0.017 \text{ km s}^{-1}$.

In the derivation of the model atmosphere parameters, small differential non-LTE corrections for the Fe I lines according to Lind et al. (2012) have been included. The largest non-LTE effects occur at the lowest gravities of the solar twin sample, i. e., $\log g \sim 4.25$; [Fe/H] is increased by 0.003 to 0.004 dex and $\log g$ by 0.007 to 0.009 dex relative to the LTE values. Changes in T_{eff} are negligible, i. e., ranging from +2 to -3 K .

The small errors quoted are only obtainable for samples of solar twin stars that can be analyzed differentially with respect

² Defined as $[\alpha/\text{Fe}] = \frac{1}{4} \cdot ([\text{Mg}/\text{Fe}] + [\text{Si}/\text{Fe}] + [\text{Ca}/\text{Fe}] + [\text{Ti}/\text{Fe}])$ in this paper.

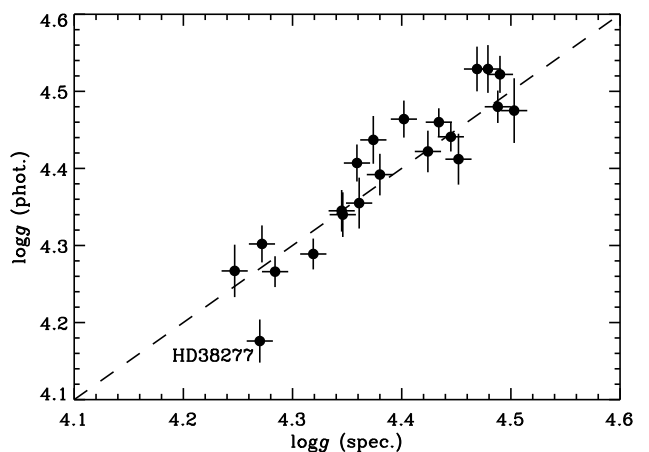


Fig. 3. Photometric gravities based on Hipparcos parallaxes as a function of spectroscopic gravities determined from the Fe ionization balance.

to the Sun using the same list of Fe lines. Still, one may wonder if these errors are really realistic. To test this, I have compared with parameters recently determined for 88 solar twin stars by Ramírez et al. (2014b) based on spectra obtained with the 6.5 m Clay Magellan Telescope and the MIKE spectrograph. The spectra have $S/N > 400$ and resolutions of $R = 83\,000$ (65 000) in the blue (red) spectral regions. A set of 91 Fe I and 19 Fe II lines were analyzed with MARCS models to derive atmospheric parameters with errors similar to those quoted above. For 14 stars in common with the present paper I get the following average differences (Ramírez – this paper) and rms deviations: $\Delta T_{\text{eff}} = 0 \pm 10 \text{ K}$, $\Delta \log g = 0.002 \pm 0.020$, and $\Delta[\text{Fe}/\text{H}] = 0.000 \pm 0.014$. The rms deviations for T_{eff} and $\log g$ are fully explainable by the errors quoted in the two works, whereas the rms deviation for [Fe/H] is a bit larger than expected.

The parameters derived in this paper are also in good agreement with those derived from HARPS spectra by Sousa et al. (2008) based on an extensive list of 236 Fe I and 36 Fe II lines analyzed by using a grid of Kurucz model atmospheres (Kurucz 1993). The average differences (Sousa – this paper) and rms deviations for the 21 solar twins in the present paper are: $\Delta T_{\text{eff}} = -1 \pm 8 \text{ K}$, $\Delta \log g = 0.018 \pm 0.033$, and $\Delta[\text{Fe}/\text{H}] = -0.003 \pm 0.009$. The deviations in T_{eff} and [Fe/H] are compatible with the small errors quoted above, but the rms deviation in $\log g$ is larger than expected; stars with $\log g < 4.35$ turn out to have systematically higher $\log g$ values in Sousa et al. (2008) than in the present paper. These deviations are not seen when comparing with $\log g$ values from Ramírez et al. (2014b).

The spectroscopic surface gravities have also been compared to photometric gravities determined from the relation

$$\log \frac{g}{g_{\odot}} = \log \frac{M}{M_{\odot}} + 4 \log \frac{T_{\text{eff}}}{T_{\text{eff},\odot}} + 0.4(M_{\text{bol}} - M_{\text{bol},\odot}), \quad (1)$$

where M is the mass of the star and M_{bol} the absolute bolometric magnitude. Hipparcos parallaxes (van Leeuwen 2007) were used to derive absolute visual magnitudes from V magnitudes based on Strömgen photometry (Olsen 1983), and bolometric corrections were adopted from Casagrande et al. (2010). Stellar masses were obtained by interpolating in the luminosity - $\log T_{\text{eff}}$ diagram between the Yonsei - Yale evolutionary tracks of Yi et al. (2003); see Nissen & Schuster (2012) for details. The estimated error of $\log g$ (phot.) ranges from 0.02 to 0.04 dex depending pri-

marily on the relative error of the parallax. As seen from Fig. 3, there is a satisfactory agreement between the two sets of gravities. The weighted mean deviation ($\log g(\text{phot.}) - \log g(\text{spec.})$) is 0.005 dex, and the rms deviation is as expected from the error bars except for one star, HD 38277, which has a 3-sigma deviation. Its lower $\log g(\text{phot.})$ could be explained if the star is a spectroscopic binary, but there is no indication of a component in the HARPS spectra.

3.3. Non-LTE and 3D effects

Although the solar twin stars have atmospheric parameters close to those of the Sun, effects of deviations from LTE may be important considering the very high precision we are aiming at.

The detailed calculations by Lind et al. (2012) show that Fe II lines are not affected by departures from LTE, but as mentioned in Sect. 3.2 there is a small non-LTE effect on Fe abundances derived from Fe I lines. Using the IDL program made available by Lind et al. to calculate non-LTE corrections for the actual set of Fe I lines applied, it is found that the largest differential correction, $\Delta[\text{Fe}/\text{H}] = 0.004$, occurs for stars having gravities about 0.15 dex below the solar gravity. Calculations of non-LTE corrections as a function of T_{eff} , $\log g$, and $[\text{Fe}/\text{H}]$ for the lines of C I (Takeda & Honda 2005), Mg I (Zhao & Gehren 2000), S I and Zn I (Takeda et al. 2005), and Ca I (Mashonkina et al. 2007), suggest similar small differential corrections as in the case of the Fe I lines; hence the non-LTE effect on the corresponding abundance ratios, $[\text{X}/\text{Fe}]$, is negligible, and the LTE ratio is therefore adopted. For the two Na I lines applied, $\lambda 6154.2$ and $\lambda 6160.7$, the calculations of Lind et al. (2011), indicate similar numerical corrections as in the case of Fe I lines, but with *opposite* sign. Therefore, non-LTE corrections have been applied when determining $[\text{Na}/\text{Fe}]$ ratios; the most extreme correction is -0.008 dex for HD 38277.

For the lines of Al I and Si I there seems to be no detailed calculations of non-LTE effects as a function of T_{eff} , $\log g$, and $[\text{Fe}/\text{H}]$ for solar type stars, but the corrections for the Sun itself are on the order of 0.01 dex only (Baumüller & Gehren 1996; Shi et al. 2008; Scott et al. 2015b). This suggests that differential corrections for the Al and Si abundances can be neglected. It is probably also the case for Ni (Scott et al. 2015a), although extensive non-LTE calculations for Ni I lines are still missing.

The statistical equilibrium calculations by Bergemann (2011) and Bergemann & Cescutti (2010) show that the Ti II and Cr II lines applied in this paper are formed in LTE in the solar atmosphere, whereas there are significant non-LTE effects for the Ti I and Cr I lines. We may investigate this empirically by comparing abundances derived from neutral and ionized lines, respectively. As seen from Fig. 4, there appears to be a trend of $[\text{Ti I}/\text{Ti II}]$ as a function of $\log g$ suggesting that solar twin stars with the lowest and highest gravities have differential non-LTE corrections on the order of ± 0.01 dex for Ti abundances derived from Ti I lines. In view of this, the Ti abundances derived from Ti II lines will be adopted although only three such lines are available compared to 11 Ti I lines. For Cr there is no significant trend of $[\text{Cr I}/\text{Cr II}]$ versus $\log g$ and the rms scatter is only 0.008 dex. In this case, the Cr abundance derived from Cr I lines is adopted.

The oxygen abundances derived from the forbidden [O I] line at 6300 Å are not affected by departures from LTE (e.g., Kiselman 1993). This line is, however, sensitive to 3D hydrodynamical (granulation) effects on the temperature structure of the stellar atmosphere (Asplund 2005). According to Nissen et

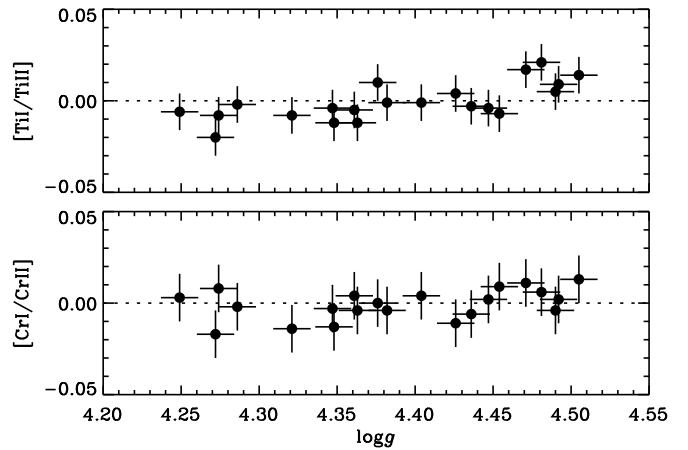


Fig. 4. The ratio of Ti abundances derived from Ti I and Ti II lines, respectively, as a function of $\log g$ (upper panel) and the corresponding ratio for Cr (lower panel).

al. (2002), this leads to 3D corrections that depend on effective temperature and metallicity. For the present sample of solar twin stars the largest differential effect on $[\text{O}/\text{H}]$ is 0.007 dex. For the other elements, one would expect 3D effects to be less significant, because the lines applied are formed deeper in the atmospheres, but this needs to be confirmed by 3D model calculations preferentially with non-LTE effects included.

The impact of magnetic fields on the temperature structure of stellar atmospheres is another potential problem. Magneto-hydrodynamic simulations of the solar atmosphere (Fabbian et al. 2010, 2012) show effects on the strength of Fe I lines induced primarily by “magnetic heating” of the upper layers. For an average vertical magnetic field strength of 100 G (Trujillo Bueno et al. 2004), the effect on the derived Fe abundance ranges from 0.01 dex for weak lines formed in deep layers to 0.08 dex for stronger lines formed in the upper part of the photosphere. These results have recently been confirmed by Moore et al. (2015), who in addition find a correction on the order of +0.02 dex for the oxygen abundance derived from the [O I] $\lambda 6300$ line if a vertical mean field of 80 G is imposed. A similar correction is suggested by the recent MHD simulations of Fabbian & Moreno-Insartis (2015).

These simulations raise the question if star-to-star differences of the magnetic field strength lead to variations of abundance ratios among solar twin stars. If so, the ratio of Fe abundances determined from Fe I and Fe II lines (used for determining the gravity parameter) would also be affected, because of different depth of formation for neutral and ionized lines. As discussed in Sect. 3.2, there is, however, good agreement between spectroscopic gravities and gravities determined via Hipparcos parallaxes, which suggests that differences in magnetic field strength do not play a major role in the context of abundance variations among solar twin stars. Still, this is a problem that deserves further studies.

3.4. Abundance ratios and uncertainties

The derived abundance ratios, $[\text{X}/\text{Fe}]$, are given in Table 3 together with the atmospheric parameters of the stars. Due to the systematic deviation between $\log g$ values derived in this paper and those of Sousa et al. (2008), four stars have gravities below the selection limit of $\log g = 4.29$.

Table 4. Uncertainties of abundance ratios.

	N_{lines}	$\sigma_{\text{atm.par.}}$ [dex]	σ_{EW} [dex]	σ_{adopted} [dex]
[C/Fe]	2	0.009	0.009	0.013
[O/Fe]	1	0.008	indv.	indv.
[Na/Fe]	2	0.002	0.004	0.007
[Mg/Fe]	2	0.002	0.010	0.011
[Al/Fe]	2	0.002	0.006	0.008
[Si/Fe]	10	0.004	0.002	0.007
[S/Fe]	4	0.009	0.012	0.016
[Ca/Fe]	7	0.002	0.003	0.006
[Ti/Fe]	3	0.007	0.007	0.010
[Cr/Fe]	10	0.001	0.003	0.006
[Ni/Fe]	14	0.001	0.003	0.006
[Zn/Fe]	3	0.004	0.009	0.011
[Y/Fe]	3	0.007	0.005	0.010

The estimated 1-sigma errors of the differential abundance ratios are given in Table 4. Column three lists the error corresponding to the uncertainty of the atmospheric parameters ($\sigma(T_{\text{eff}}) = \pm 6$ K, $\sigma(\log g) = \pm 0.012$, $\sigma([\text{Fe}/\text{H}]) = 0.006$ dex and $\sigma(\xi_{\text{turb}}) = 0.017$ km s⁻¹). For some of the abundance ratios, this error is very small, because the derived abundances of element X and Fe have almost the same dependence on the parameters. Column four lists the error arising from the measurement of equivalent widths, calculated as the line-to-line scatter of the abundances derived divided by $\sqrt{N_{\text{lines}} - 1}$, where N_{lines} is the number of spectral lines applied. In the case of oxygen for which only the weak [O I] $\lambda 6300.3$ line was used, σ_{EW} was calculated by assuming that the error of the equivalent width measurement is $\sigma(\text{EW}) = \pm 0.2$ mÅ. Finally, I have taken into account that differential 3D effects may introduce errors in the abundance ratios up to 0.005 dex. Adding these error sources in quadrature leads to the total adopted errors listed in the last column of Table 4.

4. Stellar ages

As discussed in Sect. 5, it is interesting to have information on stellar ages. Although the stars belong to the main sequence, relative ages may be derived from the precise values of T_{eff} and $\log g$ as shown in Fig. 5, where the stars are compared to a Yonsei-Yale set of isochrones (Yi et al. 2001; Kim et al. 2002). Using the IDL program made available by Kim et al. to calculate isochrones for the actual combination of $[\text{Fe}/\text{H}]$ and $[\alpha/\text{Fe}]$ for a given star, it is possible to interpolate to the stellar age and its internal 1-sigma error. The results are given in Table 5 together with stellar masses derived from T_{eff} and $\log g$. The internal error of the mass is on the order of $\pm 0.01 M_{\text{sun}}$.

As seen from Fig. 6, the stellar ages agree very well with the values of Ramírez et al. (2014b), who also determined ages from Yonsei-Yale isochrones in the $T_{\text{eff}} - \log g$ diagram. The small systematic deviation for the three oldest stars may be due to the fact that they have enhanced $[\alpha/\text{Fe}]$ values ($[\alpha/\text{Fe}] \approx 0.08$), which were taken into account when deriving their ages in the present paper, but apparently not by Ramírez et al. (2014b).

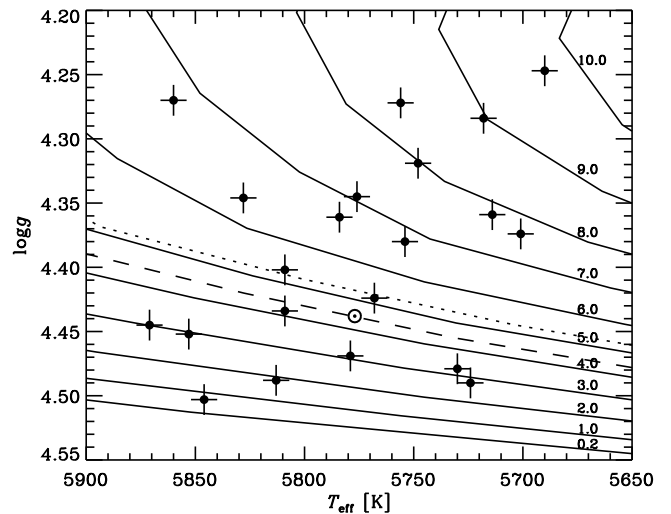


Fig. 5. The $T_{\text{eff}} - \log g$ diagram of solar twin stars in comparison with Yonsei-Yale isochrones corresponding to ages given to the right in Gyr. The isochrones refer to $[\text{Fe}/\text{H}] = 0.0$ and $[\alpha/\text{Fe}] = 0.0$, but 5 Gyr isochrones corresponding to $[\text{Fe}/\text{H}] = -0.05$ (dashed line) and $[\alpha/\text{Fe}] = +0.1$ (dotted line) are also shown. The position of the Sun with an age of 4.55 Gyr is marked.

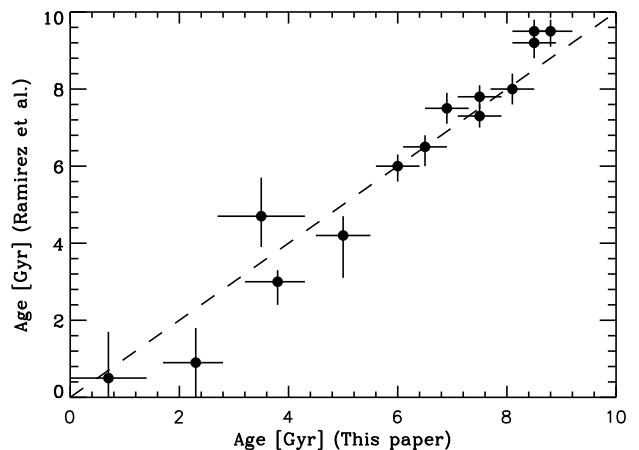


Fig. 6. Comparison of stellar ages derived in this paper with ages determined by Ramírez et al. (2014b).

5. Discussion

5.1. $[\text{X}/\text{Fe}]$ - stellar age correlations

As seen from Fig. 7, the dispersion of $[\text{X}/\text{Fe}]$ at a given $[\text{Fe}/\text{H}]$ is larger than expected from the estimated error bars except in the case of [Cr/Fe]. Three stars (HD 45289, HD 210918, and HD 220507) marked by open (red) squares stand out by having high $[\text{X}/\text{Fe}]$ ratios of the alpha-capture elements O, Mg, Si, S, and Ti, and are also high in C, Al, and Zn. These stars probably belong to the class of metal-rich α -enhanced stars first identified by Adibekyan et al. (2011; 2012) as a population having $[\alpha/\text{Fe}] \approx +0.1$ in contrast to normal thin-disk stars with $[\alpha/\text{Fe}] \approx +0.0$. Bensby et al. (2014) confirm the existence of such metal-rich α -enhanced stars, and Haywood et al. (2013) show that they belong to a thick-disk sequence in the $[\alpha/\text{Fe}] - [\text{Fe}/\text{H}]$ diagram for which the ages range from ~ 13 Gyr at

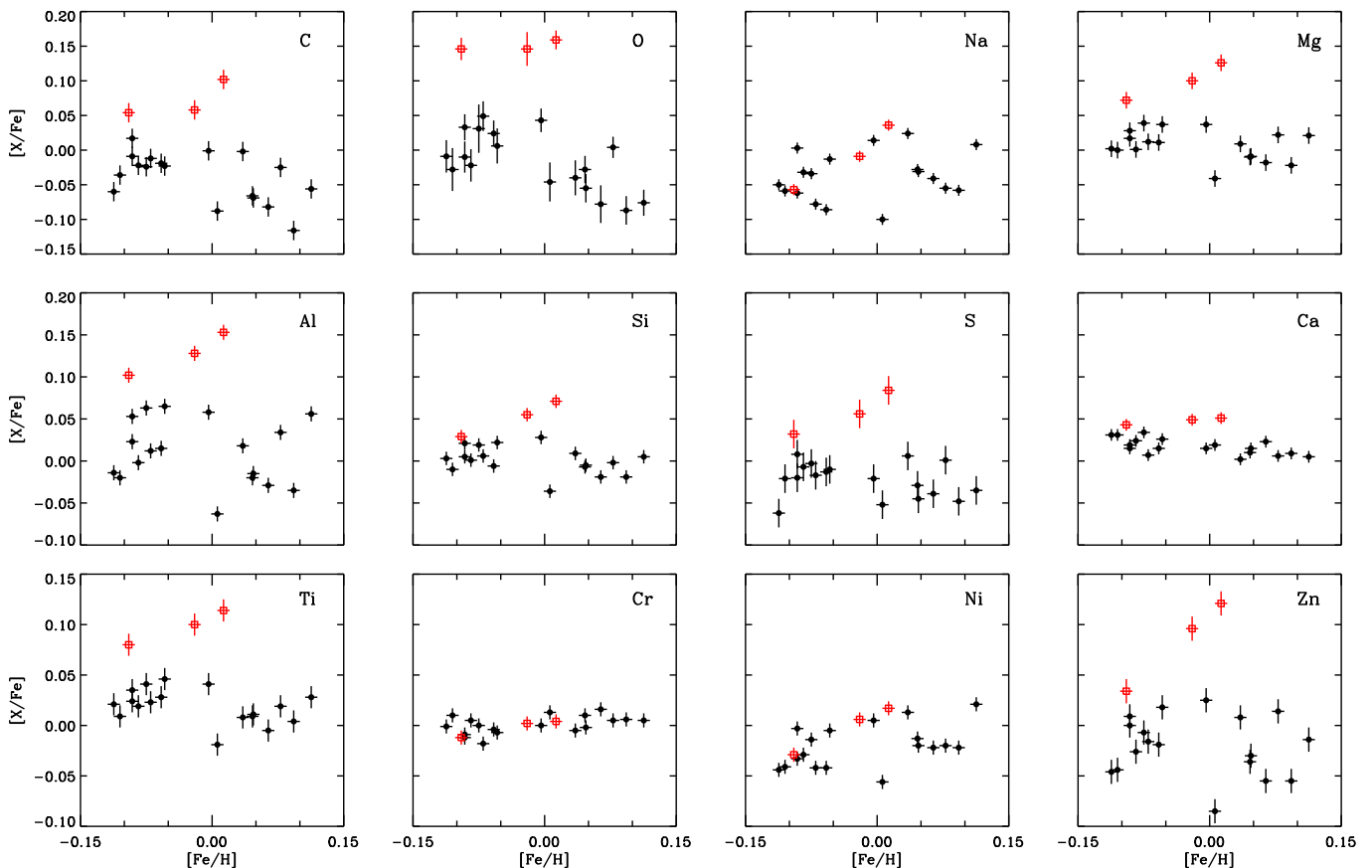


Fig. 7. Abundance ratios $[X/Fe]$ as a function of $[Fe/H]$. The error bars shown correspond to the errors listed in Table 4. Open (red) squares: α -enhanced stars. Filled circles: thin-disk stars

$[Fe/H] = -1$ to ~ 8 Gyr at $[Fe/H] = +0.2$. The ages of the three α -enhanced stars found in this paper (8 - 9 Gyr) agree with this interpretation. Furthermore, two of the α -enhanced stars (HD 45289 and HD 210918), have thick-disk kinematics according to the Galactic velocity components given in Adibekyan et al. (2012). The third one has typical thin-disk kinematics like the rest of the sample.

Even if we exclude the three α -enhanced stars, there are still variations in the abundance ratios that cannot be explained by the estimated errors of the determinations. Interestingly, there is a clear correlation between $[X/Fe]$ and stellar age for most of the elements as seen from Fig. 8. Linear fits ($[X/Fe] = a + b \cdot \text{Age}$) have been obtained by a maximum likelihood program that includes errors in both coordinates. Coefficients a and b are given in Table 6 together with standard deviations and reduced chi-squares of the fits. As seen, $[Mg/Fe]$, $[S/Fe]$, $[Ti/Fe]$, and $[Cr/Fe]$ are very well correlated with age ($\chi_{\text{red}}^2 \sim 1$), but $[C/Fe]$, $[O/Fe]$, $[Al/Fe]$, $[Si/Fe]$, $[Cr/Fe]$, and $[Zn/Fe]$ also show a clear dependence on age. Exceptions are $[Na/Fe]$ and $[Ni/Fe]$, which will be discussed below.

Figure 9 (lower panel) shows how astonishingly well $[Mg/Fe]$ for thin-disk stars is correlated with age in contrast to the lack of correlation between $[Fe/H]$ and age (upper panel). Given that Type Ia Supernovae (SNe) provide about two-thirds of Fe in the Galactic disk but very little Mg (Kobayashi et al.

2006), the age correlation of $[Mg/Fe]$ can be explained by an increasing number of Type Ia SNe relative to the number of Type II SNe as time goes on. The small scatter in the $[Mg/Fe]$ -age relation then indicates that nucleosynthesis products of Type Ia and Type II SNe are well mixed locally in the Galactic disk before new stars are formed. The large scatter in metallicity ($\sigma[Fe/H] \approx 0.07$ dex) at a given age may be explained by infall of metal-poor gas onto the Galactic disk followed by star formation before mixing evens out the chemical inhomogeneities. The infalling gas will mainly contribute hydrogen causing a decrease of $[Fe/H]$ but leave $[Mg/Fe]$ unaffected. This scenario is discussed in detail by Edvardsson et al. (1993), who were first to discover the large spread in the age-metallicity relation of thin-disk stars in contrast to a small spread in $[\alpha/Fe]$, but their precision of abundance ratios (typically ± 0.05 dex)³ was not high enough to see a correlation between $[\alpha/Fe]$ and stellar age. Alternatively, the dispersion in $[Fe/H]$ at a given age may be related to orbital mixing of stars born at different galactocentric distances (R_G) provided that there is a strong radial gradient in $[Fe/H]$ around the solar distance (Haywood et al. 2013), but then the very small dispersion in $[X/Fe]$ at a given age requires that the star formation history is independent of R_G (Haywood et al. 2015).

³ The Edvardsson et al. sample is not limited to solar twin stars and abundances were derived from high-resolution spectra with $S/N \sim 200$.

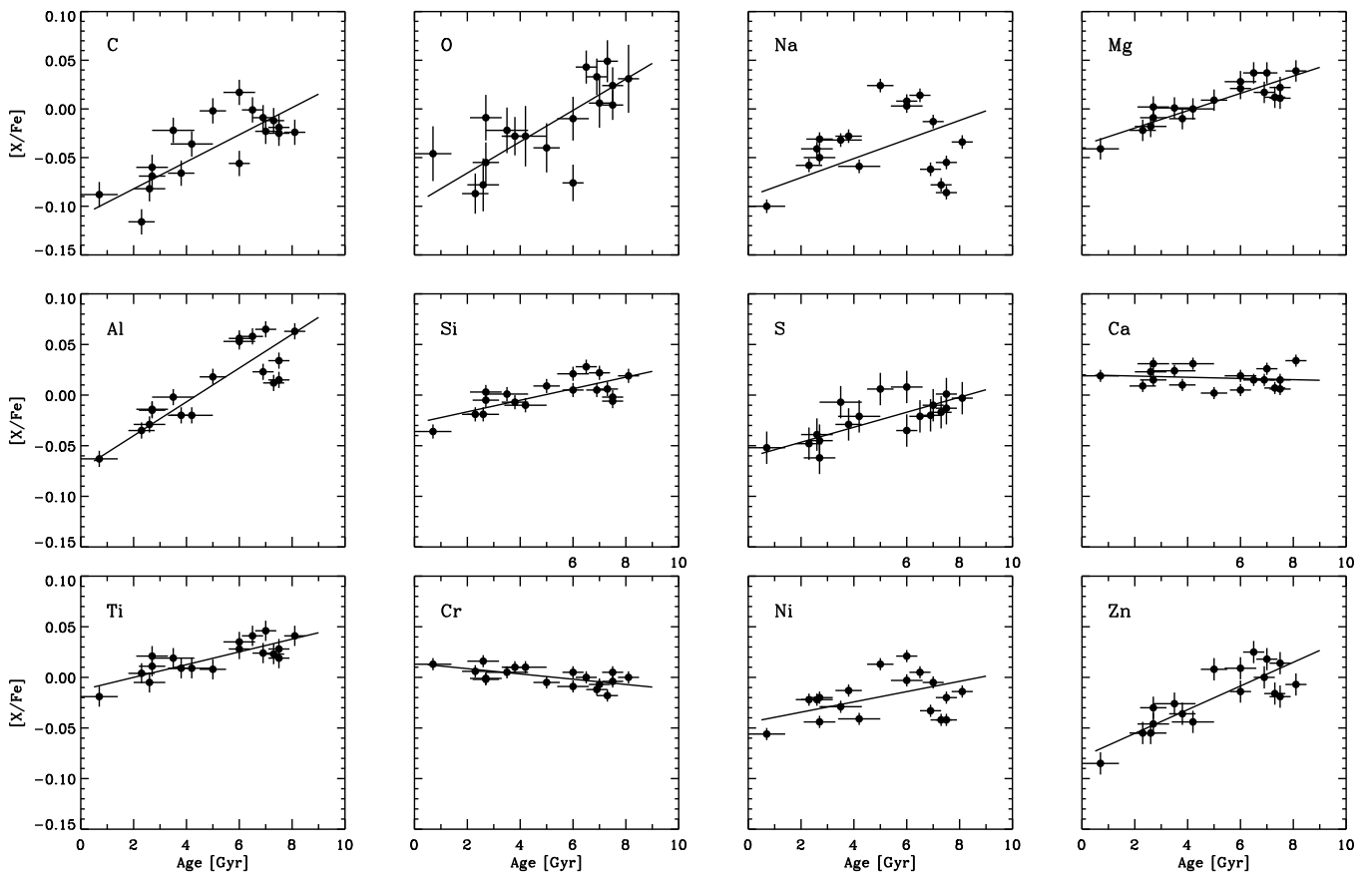


Fig. 8. Abundance ratios $[X/Fe]$ as a function of stellar age for the thin-disk stars. The lines show maximum likelihood linear fits to the data, with zero points and slope coefficients as given in Table 6.

As seen from Fig. 8 and Table 6, the slope of $[X/Fe]$ versus age differs from element to element. To some extent this may be explained in terms of differences in the relative contributions of Type Ia and Type II SNe to the various elements, but it cannot explain that the age-slopes for C, O, and Al are significantly larger than that of Mg, because for all four elements, the yield of Type Ia SNe is negligible compared to the Type II SNe yield (e.g., Kobayashi et al. 2006). Hence, it seems that one has to include an evolving initial mass function to explain the age trends seen in Fig. 8. Asymptotic giant branch (AGB) stars (Karakas 2010) should also be considered, but cannot solve the problem; they contribute C and Al (as well as Na) but no Fe, and hence *increase* $[X/Fe]$ for these elements as a function of increasing time, i.e., decreasing stellar age.

The near-constancy of $[Ca/Fe]$ as a function of stellar age (see Fig. 8) is another puzzling problem. According to yields of supernovae (Kobayashi et al. 2006), one would expect $[Ca/Fe]$ to increase with age in the same way as $[Si/Fe]$ and $[S/Fe]$. A similar problem is encountered in studies of abundance ratios in early-type galaxies (Conroy et al. 2014); $[Ca/Fe]$ is constant as a function of stellar velocity dispersion in contrast to a rising trend for the other α -capture elements. Mulchaey et al. (2014) suggest that this special behavior of Ca as well as the high Ca abundance in diffuse gas of clusters of galaxies is due to a new class of low luminosity supernovae exemplified by SN 2005E, for which the amount of synthesized Ca is 5-10 times greater than that of

classical Type Ia SNe (Perets et al. 2010). Perhaps these Ca-rich SNe are also important for the chemical evolution of the Galactic disk.

Diffusion of elements (gravitational settling and radiative levitation) should also be considered when discussing abundances of stars as a function of time. Helioseismology and models of the Sun indicate that the surface abundances of heavy elements (and helium) have decreased by $\sim 10\%$ relative to their initial values (Christensen Dalsgaard et al. 1996). According to Turcotte & Wimmer-Schweingruber (2002), the effect on $[X/Fe]$ is, however, much smaller, i.e., < 0.004 dex for the elements discussed in this paper. This means that diffusion can be neglected when discussing the age trends of $[X/Fe]$.

The *s*-process element yttrium is not included in Fig. 8, but in contrast to most of the other elements, $[Y/Fe]$ decreases with stellar age as previously found for barium (Edvardsson et al. 1993; Bensby et al. 2007). This is probably due to an increasing contribution of Y and Ba from low-mass ($1-4 M_{\text{Sun}}$) AGB stars as time goes on (Travaglio et al. 2004). As the slope of $[Y/Fe]$ versus age is quite steep ($b = -0.033$ dex Gyr^{-1} with opposite sign to that of $[Mg/Fe]$ ($b = +0.009$ dex Gyr^{-1}), $[Y/Mg]$ becomes a sensitive indicator of age as seen from Fig. 10. A maximum likelihood fit to the data yields the relation

$$[Y/Mg] = 0.175 (\pm 0.011) - 0.0404 (\pm 0.0019) \text{ Age [Gyr]} \quad (2)$$

with $\chi_{\text{red}}^2 = 0.71$.

Table 5. Stellar ages and masses.

Star	Age [Gyr]	Mass [M_{\odot}]	Note ^a
HD 2071	3.5 ± 0.8	0.97	
HD 8406	4.2 ± 0.8	0.96	
HD 20782	7.5 ± 0.4	0.97	1.8 M_J ^b
HD 27063	2.6 ± 0.6	1.04	
HD 28471	7.0 ± 0.4	0.97	
HD 38277	7.3 ± 0.4	1.01	
HD 45184	2.7 ± 0.5	1.06	0.04 M_J ^c
HD 45289*	8.5 ± 0.4	1.00	
HD 71334	8.1 ± 0.4	0.94	
HD 78429	7.5 ± 0.4	1.04	
HD 88084	6.0 ± 0.6	0.96	
HD 92719	2.7 ± 0.6	0.99	
HD 96116	0.7 ± 0.7	1.05	
HD 96423	6.0 ± 0.4	1.03	
HD 134664	2.3 ± 0.5	1.07	
HD 146233	3.8 ± 0.5	1.04	
HD 183658	5.0 ± 0.5	1.03	
HD 208704	6.9 ± 0.4	0.98	
HD 210918*	8.5 ± 0.4	0.96	
HD 220507*	8.8 ± 0.4	1.01	
HD 222582	6.5 ± 0.4	1.01	7.8 M_J ^d

Notes. ^(*) α -enhanced star. ^(a) Mass of detected planet in units of Jupiter's mass. ^(b) Jones et al. (2006). ^(c) Mayor et al. (2011). ^(d) Butler et al. (2006).

Table 6. Linear fits of $[X/Fe]$ as a function of stellar age.

	a [dex]	b 10^{-3} dex Gyr ⁻¹	$\sigma[X/Fe]^a$ [dex]	χ^2_{red}
[C/Fe]	-0.110 ± 0.011	+13.9 ± 2.0	0.025	2.7
[O/Fe]	-0.098 ± 0.015	+16.1 ± 2.8	0.030	1.9
[Na/Fe]	-0.090 ± 0.035	+9.8 ± 6.3	0.039	20.6
[Mg/Fe]	-0.037 ± 0.005	+8.9 ± 0.9	0.011	0.8
[Al/Fe]	-0.074 ± 0.011	+16.7 ± 1.9	0.020	3.6
[Si/Fe]	-0.028 ± 0.005	+5.7 ± 0.9	0.012	2.4
[S/Fe]	-0.058 ± 0.007	+7.0 ± 1.3	0.015	0.8
[Ca/Fe]	+0.020 ± 0.004	-0.6 ± 0.8	0.010	2.7
[Ti/Fe]	-0.013 ± 0.005	+6.3 ± 0.8	0.010	0.9
[Cr/Fe]	+0.014 ± 0.003	-2.6 ± 0.6	0.007	1.4
[Ni/Fe]	-0.044 ± 0.011	+4.8 ± 2.0	0.021	10.7
[Zn/Fe]	-0.079 ± 0.008	+11.7 ± 1.4	0.018	2.0
[Y/Fe]	+0.146 ± 0.011	-33.0 ± 2.0	0.023	1.6

Notes. ^(a) Standard deviation of $[X/Fe]$ for the linear fit.

For elements having a condensation temperatures markedly different from that of Fe, the variations in the $[X/Fe]-T_C$ slope discussed in Sect. 5.2 contribute to the scatter in the $[X/Fe]$ -age relation. In particular, this effect may explain why the scatter in $[C/Fe]$ and $[O/Fe]$ is larger than expected from the estimated errors of the determinations, i.e., $\chi^2_{\text{red}} = 2.7$ and 1.9, respectively. $[C/O]$, on the other hand, is not much affected by the $[X/Fe]-T_C$ slope variations, because the two elements have similar low condensation temperatures.

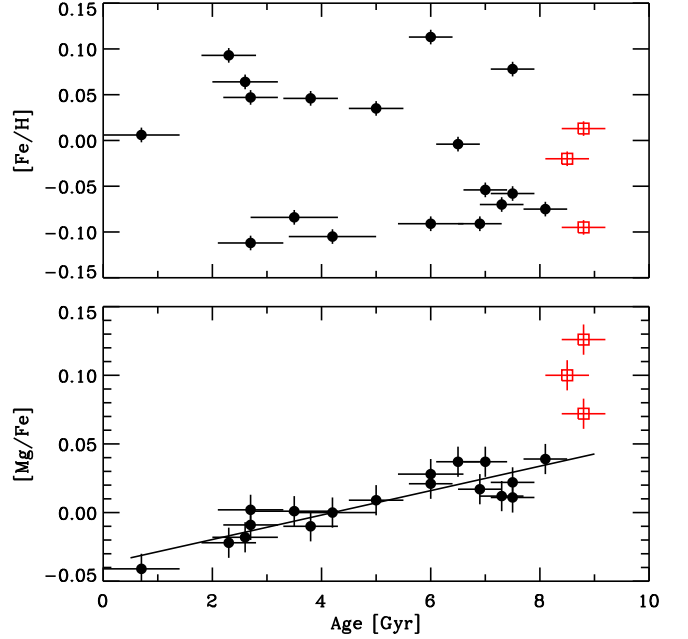


Fig. 9. $[Fe/H]$ and $[Mg/Fe]$ versus stellar age. Thin-disk stars are shown with filled circles and α -enhanced stars with open (red) squares. The line in the lower panel corresponds to the fit given in Table 6.

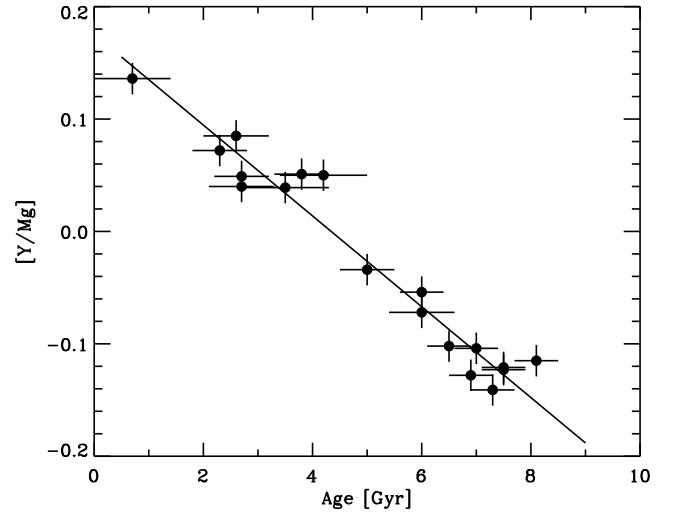


Fig. 10. $[Y/Mg]$ versus stellar age for thin-disk stars.

Recently, the C/O ratio⁴ in solar-type stars has been much discussed, mainly because its value may influence the composition of planets formed in circumstellar disks (e.g., Bond et al. 2010; Fortney 2012; Gaidos 2015). In some studies (Delgado Mena et al. 2010; Petigura & Marcy 2011), C/O was found to range from ~ 0.4 to $\gtrsim 1.0$, i.e., up to a factor of two higher than the solar ratio, $C/O_{\odot} = 0.55 \pm 0.10$ (Asplund et al. 2009;

⁴ C/O is defined as N_C/N_O , where N_C and N_O are the number densities of carbon and oxygen nuclei, respectively, and should not be confused with the solar-normalized logarithmic ratio, $[C/O]$.

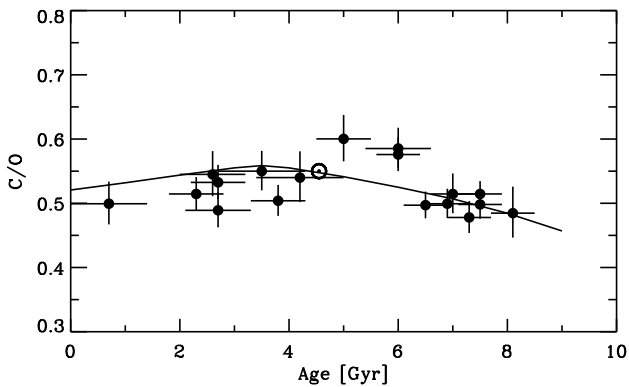


Fig. 11. The C/O ratio as a function of stellar age. The line shows the evolution of C/O (normalized to a solar ratio of 0.55) according to the chemical evolution calculations of Gaidos (2015).

Caffau et al. 2011). This has led to speculations about the existence of exoplanets consisting of carbides and graphite instead of Earth-like silicates (Bond et al. 2010). Alternative determinations of C/O in solar-type stars (Nissen 2013; Nissen et al. 2014; Teske et al. 2014) show, however, only a small scatter in C/O and an increasing trend as a function of [Fe/H] reaching $C/O \approx 0.8$ at $[Fe/H] \approx 0.4$. The scatter of C/O for the solar twin stars is also small, i.e., ± 0.035 only around a mean value of $\langle C/O \rangle = 0.52$ (see Fig. 11). Furthermore, there is not much evolution of C/O as a function of time despite the fact that both C/Fe and O/Fe evolve significantly. This agrees very well with the recent Galactic chemical evolution calculations of Gaidos (2015) as seen from Fig. 11. In his model, the dominant contribution of C and O comes from massive stars, and C/O has only a moderate rise during the first ~ 5 Gyr due to an increasing contribution of carbon from stars of lower mass.

As mentioned above, [Na/Fe] and [Ni/Fe] are not well correlated with stellar age; according to Table 6 the linear fits have $\chi_{\text{red}}^2 > 10$. Curiously, there is, however, a tight correlation between [Na/Fe] and [Ni/Fe] as shown in Fig. 12. A maximum likelihood linear fit with errors in both coordinates provides the relation

$$[Ni/Fe] = 0.002 (\pm 0.002) + 0.580 (\pm 0.032) [Na/Fe] \quad (3)$$

with a standard deviation $\sigma[Ni/Fe] = 0.008$, which is close to that expected from the estimated errors of [Na/Fe] and [Ni/Fe], i. e., ± 0.007 and ± 0.006 dex, respectively.

Apparently, correlated variations of [Ni/Fe] and [Na/Fe] among solar-metallicity stars have not been noted before. This is understandable given that the amplitude is small, i.e., ~ 0.07 dex in [Ni/Fe]; it requires very high abundance precision to see the variations⁵. A Ni-Na relation has, however, been found for thick-disk and halo stars with $-1.6 < [Fe/H] < -0.4$ (Nissen & Schuster 1997, 2010, 2011) and for stars in dwarf spheroidal galaxies in the same metallicity interval (Venn et al. 2004; Letarte 2010; Lemasle 2014). For these metal-poor stars, the amplitude of the variations is larger (~ 0.3 dex in [Ni/Fe]), but the slope of the [Ni/Fe] - [Na/Fe] relation is about the same as found for the solar-metallicity stars, i. e. $\Delta[Ni/Fe]/\Delta[Na/Fe] \approx 0.5$. Furthermore, the lowest Ni/Fe and Na/Fe ratios are found among

⁵ For the solar twin stars studied, abundance ratios derived from HARPS spectra by Neves et al. (2009) show in fact correlated variations in [Ni/Fe] and [Na/Fe] similar to Fig. 12, but it was not noted in that paper nor in subsequent papers based on HARPS spectra.

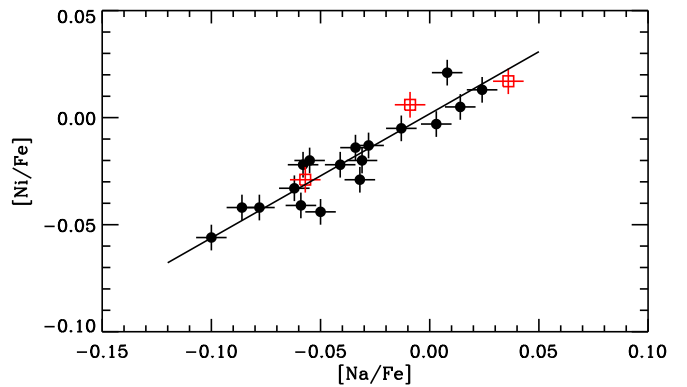


Fig. 12. [Ni/Fe] versus [Na/Fe] with the same symbols as used in Fig. 7. The line corresponds to the linear fit of [Ni/Fe] as a function of [Na/Fe] given in Eq. (2).

stars with the lowest α/Fe ratios, which agrees with the trends seen for the solar twin stars.

As discussed by Venn et al. (2004), the Ni-Na correlation may be due to the fact that the yields of Na and the dominant isotope of Ni (Ni^{58}) produced in massive stars exploding as Type II SNe both depend on the neutron excess, which itself depends on metallicity and the α/Fe ratio. Neutrons are released by the $^{22}Ne(\alpha, n)^{25}Mg$ reaction, where ^{22}Ne comes from double α -capture on ^{14}N made from initial C and O in the CNO cycle. It is, however, difficult to understand why [Na/Fe] and [Ni/Fe] are not well correlated with stellar age like the other abundance ratios; it was argued above that α -capture elements produced in Type II SNe must be efficiently mixed in interstellar gas to explain the small scatter of [Mg/Fe] at a given age, so why should there be variations of the neutron excess?

5.2. [X/Fe]- T_C correlations

As discussed in Sect. 1, sequestration of refractory elements in terrestrial planets or on interstellar dust particles may introduce star-to-star differences of abundance ratios, which are correlated with elemental condensation temperature T_C (Lodders 2003). In order to see if this is the case, [X/Fe] has been plotted as a function of T_C for all stars and linear-least squares fits with [X/Fe] weighted by the inverse square of its error have been obtained. The coefficients and the reduced χ^2 of the fits are given in Table 7. Figure 13 shows some typical examples⁶.

As seen from Table 7, the reduced χ^2 of the fits is larger than one for all stars indicating that there is never a perfect correlation between [X/Fe] and T_C . Nevertheless, for several stars the slope coefficient is more than three times larger than the error of the slope. The first star, HD 134664, in Fig. 13 with a slope $\Delta[X/Fe]/\Delta T_C = 6.7 \pm 1.6 \times 10^{-5} \text{ dex K}^{-1}$ represents such a case. It has a ratio between refractory elements with $T_C > 1200$ K and the volatile elements C and O about 0.08 dex higher than in the Sun. Assuming that HD 134664 has a pristine composition, this means that the Sun has been depleted in refractory elements by as much as 20% as first advocated by Meléndez et al. (2009) from abundance ratios in 11 solar twins.

The second star in Fig. 13, HD 146233 (18 Sco) represents an intermediate case with $\Delta[X/Fe]/\Delta T_C = 3.8 \pm 1.1 \times 10^{-5} \text{ dex K}^{-1}$. This star has recently been studied in detail by Meléndez et al.

⁶ Yttrium is not included in the [X/Fe]- T_C fits, because for many stars [Y/Fe] has a large deviation.

Table 7. Linear fits, $[X/Fe] = a + b \cdot T_C$.

Star	a [dex]	b [10^{-5} dex K^{-1}]	χ_{red}^2
HD 2071	-0.043 ± 0.019	3.1 ± 1.5	4.9
HD 8406	-0.068 ± 0.030	4.4 ± 2.3	11.2
HD 20782	-0.060 ± 0.034	3.7 ± 2.6	16.3
HD 27063	-0.084 ± 0.023	5.5 ± 1.8	6.8
HD 28471	-0.041 ± 0.023	4.3 ± 1.8	6.8
HD 38277	-0.051 ± 0.034	2.9 ± 2.6	14.8
HD 45184	-0.069 ± 0.013	4.6 ± 1.0	2.2
HD 45289*	$+0.021 \pm 0.052$	1.9 ± 4.0	35.1
HD 71334	-0.059 ± 0.026	5.5 ± 2.0	8.3
HD 78429	-0.038 ± 0.024	2.8 ± 1.8	8.4
HD 88084	-0.011 ± 0.019	1.9 ± 1.5	5.0
HD 92719	-0.081 ± 0.027	5.4 ± 2.1	9.9
HD 96116	-0.113 ± 0.042	6.1 ± 3.2	21.7
HD 96423	-0.060 ± 0.015	5.5 ± 1.1	3.1
HD 134664	-0.106 ± 0.020	6.7 ± 1.6	5.6
HD 146233	-0.058 ± 0.014	3.8 ± 1.1	2.7
HD 183658	$+0.003 \pm 0.012$	0.4 ± 0.9	1.7
HD 208704	-0.041 ± 0.029	2.7 ± 2.2	11.5
HD 210918*	$+0.003 \pm 0.056$	1.4 ± 4.3	46.2
HD 220507*	$+0.085 \pm 0.053$	-1.7 ± 4.1	43.9
HD 222582	-0.002 ± 0.019	1.7 ± 1.5	5.4

Notes. (*) α -enhanced star.

(2014a), who for 20 elements with $Z \leq 30$ find a T_C -slope of 3.5×10^{-5} dex K^{-1} in excellent agreement with the value found in this paper⁷. Neutron capture elements were, however, found to have higher abundances than expected from the $[X/Fe]$ - T_C relation. This is confirmed by deriving abundances of Y, Ba and Eu from the HARPS spectrum of HD 146233.

The third star in Fig. 13, HD 183658, is the only one in the sample with a well-defined relation between $[X/Fe]$ and T_C and a slope close to zero. Thus, it is the only star for which the $[X/Fe]$ distribution matches that of the Sun, confirming that the Sun is unusual among solar twin stars.

For the three α -enhanced stars, there is no correlation between $[X/Fe]$ and T_C as shown in the case of HD 210918 in the last panel of Fig. 13. In addition, there are five stars with $\chi_{\text{red}}^2 > 10$ for which the correlation is also poor, mainly because $[Na/Fe]$ and $[Ni/Fe]$ deviate strongly from the mean trend. As shown in Fig. 13 for the case of HD 20782 very different slopes are derived depending on whether one includes all elements or fit only elements with a condensation temperature $T_C > 900$ K as in Ramírez et al. (2009). Another solar twin (HIP 102152) with deviating $[Na/Fe]$ and $[Ni/Fe]$ values was analyzed by Monroe et al. (2013), who suggest that the low sodium (and nitrogen) abundance could be due to its high age (8 Gyr). However, stars with low Na and Ni abundances in this paper cover a broad range in age. Instead, it should be noted that HIP 102152 with $[Na/Fe] = -0.044$ and $[Ni/Fe] = -0.026$ according to Monroe et al. fits the Ni-Na relation shown in Fig. 12 almost exactly.

Recently, Adibekyan et al. (2014) have found evidence for a dependence of the $[X/Fe]$ - T_C slope on stellar age using data based on HARPS spectra for 148 solar-like stars with $5600 < T_{\text{eff}} < 6375$ K, $4.10 < \log g < 4.65$ and $-0.3 < [Fe/H] < +0.4$. For this sample, the T_C -slope changes by about 6×10^{-5} dex K^{-1}

⁷ For 13 elements in common, the mean deviation and rms scatter for HD 146233 are $\Delta[X/H]$ (Melendez – this paper) = 0.003 ± 0.007 dex confirming the high precision estimated in the two papers.

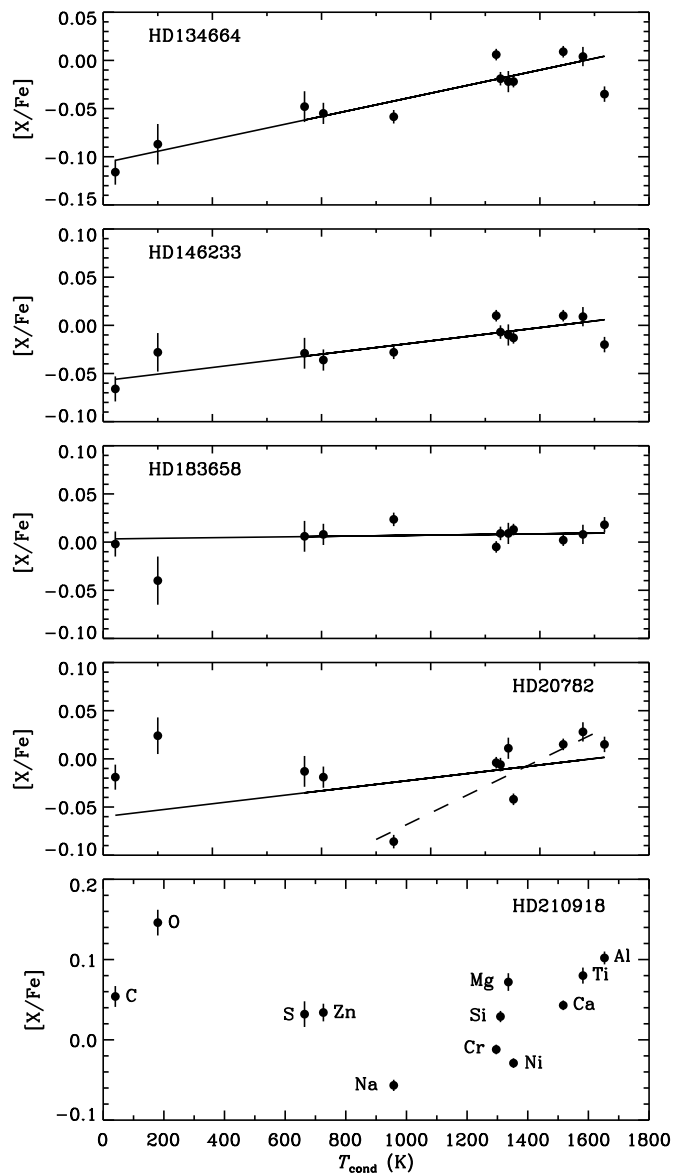


Fig. 13. The relation between $[X/Fe]$ and elemental condensation temperature (Lodders 2003) for five representative stars. The lines show linear fits to the weighted values of $[X/Fe]$. In the case of HD 20782, the dashed line shows the fit for elements with $T_C > 900$ K.

for an age change of 10 Gyr. A similar age dependence of the $[X/Fe]$ - T_C slope were found for a group of 59 metal-rich solar-analog stars by Ramírez et al. (2014a). As seen from Fig. 14, there is also evidence for an age dependence of the slopes derived in this paper. From a maximum likelihood fit to the data for the thin-disk stars I get

$$b = 5.6(\pm 0.8) - 0.43(\pm 0.15) \text{ Age [Gyr]}, \quad (4)$$

where b is the $[X/Fe]$ versus T_C slope in units of 10^{-5} dex K^{-1} . The fit has a satisfactory $\chi_{\text{red}}^2 = 1.5$, but one star, HD 183658, and the Sun have a 3-sigma deviation. Within the errors, the change of the T_C -slope with age agrees with the result of Adibekyan et al.⁸. Furthermore, it is noted that the change in T_C -slope is

⁸ Note that Adibekyan et al. (2014) define the T_C -slope with the opposite sign of that used in the present paper.

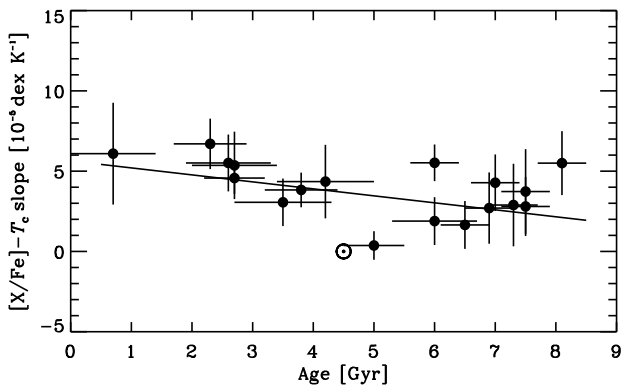


Fig. 14. The relation between the $[X/Fe]-T_C$ slope and stellar age for thin-disk stars. The line shows the fit given in Eq. (3).

mainly caused by the fact that the change of $[C/Fe]$ and $[O/Fe]$ with age is steeper than the corresponding change for refractory elements.

6. Summary and conclusions

In this paper, HARPS spectra with $S/N \geq 600$ have been used to derive very precise atmospheric parameters ($\sigma(T_{\text{eff}}) \approx 6\text{ K}$; $\sigma(\log g) \approx 0.012$) and elemental abundances for a sample of 21 solar twin stars in the solar neighborhood. Small differential non-LTE effects were taken into account when determining $[Na/Fe]$ ratios and estimated to be negligible for the other abundance ratios derived. Differential 3D effects seem to be unimportant, although the impact of possible variations in the magnetic field strength deserves further studies. Altogether, the error of the abundance ratios derived is estimated to be on the order of ± 0.01 dex. This high precision is supported by comparing abundances of HD 146233 (18 Sco) with those determined by Meléndez et al. (2014a) from UVES spectra.

In addition, precise stellar ages are obtained by interpolating between Yonsei-Yale isochrones in the $\log g-T_{\text{eff}}$ diagram. A comparison with ages derived by Ramírez et al. (2014b) indicates that the ages have internal errors ranging from 0.4 to 0.8 Gyr.

It is confirmed that the Sun has a lower ratio between refractory and volatile elements than the large majority of solar twin stars as found by Meléndez et al. (2009). Only one star (HD 183658) has the same relation between $[X/Fe]$ and elemental condensation temperature T_C as the Sun. For several of the other stars, there is a positive correlation between $[X/Fe]$ and T_C with slope coefficients ranging by more than a factor of two. This may be explained by various degrees of sequestration of refractory elements on terrestrial planets (Meléndez et al. 2009) or by dust-gas segregation in circumstellar disks (Gaidos 2015).

For most of the solar twins, the correlation between $[X/Fe]$ and T_C is rather poor, i.e., $\chi_{\text{red}}^2 > 1$ for the linear fits. For many of the elements there is, on the other hand, an astonishingly tight correlation between $[X/Fe]$ and stellar age with amplitudes up to ~ 0.15 dex over an age interval of 8 Gyr. These age correlations may be related to an increasing number of Type Ia SNe relative to the number of Type II SNe as time goes on and/or an evolving initial mass function in the Galactic disk. If so, the slopes of the age relations for the various elements provide new constraints on supernovae yields and Galactic chemical evolution. Furthermore, the small scatter of $[X/Fe]$ in the age relations suggests that nucleosynthesis products of SNe are well

mixed locally before new generations of stars are formed. In contrast, there is a large scatter of $[Fe/H]$ at a given age, which may be explained by infall of metal-poor gas clouds followed by star formation before mixing evens out the inhomogeneities (Edvardsson et al. 1993).

$[Ca/Fe]$ is nearly constant as a function of stellar age in contrast to an increasing $[X/Fe]$ for the other α -capture elements. This cannot be explained by yields calculated for supernovae of Types II and Ia, and perhaps it indicates that the new class of low-luminosity Ca-rich supernovae discussed by Perets et al. (2010) play an important role for the chemical evolution of the Galactic disk.

$[Y/Mg]$ appears to be a sensitive chronometer for Galactic evolution as seen from Fig. 10. If $[Y/Mg]$ can be measured with a precision of 0.04 dex, the age of solar metallicity stars can be estimated from Eq. (2) with a precision of 1 Gyr, but further studies are needed to see how this relation depends on $[Fe/H]$.

The C/O ratio is found to evolve very little over the life time of the Galactic disk, i.e., to lie within ± 0.04 from the solar value of $C/O \approx 0.55$; in contrast $[C/Fe]$ and $[O/Fe]$ change by ~ 0.15 dex. This is of particular interest for discussions of compositions of exoplanets, because C/O is a key determinant for the composition of solids that condense from gas in circumstellar disks.

Na and Ni are exceptions to the tight correlation between $[X/Fe]$ and stellar age, but interestingly there is a strong correlation between $[Ni/Fe]$ and $[Na/Fe]$ with a slope of ≈ 0.6 and an amplitude of ~ 0.07 dex in $[Ni/Fe]$. A similar Ni-Na relation has previously been found for more metal-poor halo stars (Nissen & Schuster 1997, 2010) and has been ascribed to the fact that the yields of Na and Ni produced in massive stars and expelled by Type II SNe both depend on the neutron excess. It is, however, difficult to understand why $[Na/Fe]$ and $[Ni/Fe]$ are not well correlated with stellar age like the other abundance ratios.

The changes of $[X/Fe]$ with stellar age and the correlated variations of $[Ni/Fe]$ and $[Na/Fe]$ among solar twin stars complicate the use of the $[X/Fe]-T_C$ slope as a possible signature of terrestrial planets around stars. Altogether, the interpretation of abundance ratios in solar twin stars, when determined with a precision of ~ 0.01 dex, is difficult, because $[X/Fe]$ seems to be affected both by planet formation or dust-gas segregation and chemical evolution in the Galactic disk. Further studies of high-precision differential abundances for solar twins and stars with other metallicities including wide binaries are needed.

Acknowledgements. Funding for the Stellar Astrophysics Centre is provided by the Danish National Research Foundation (Grant agreement no.: DNR106). The research is supported by the ASTERISK project (ASTERoseismic Investigations with SONG and Kepler) funded by the European Research Council (Grant agreement no.: 267864). An anonymous referee as well as Vardan Adibekyan, Martin Asplund, Karsten Brogaard, Jonay González Hernández, Bengt Gustafsson, Jorge Meléndez, Ivan Ramírez, and David Yong are thanked for important comments on a first version of the manuscript. Karin Lind is thanked for IDL programs to calculate non-LTE corrections for abundances derived from Na I and Fe I lines. This research made use of the SIMBAD database operated at CDS, Strasbourg, France.

References

- Adibekyan, V. Zh., González Hernández, J. I., Delgado Mena, E., et al. 2014, *A&A*, 564, L15
- Adibekyan, V. Zh., Santos, N. C., Sousa, S. G., & Israelian, G. 2011, *A&A*, 535, L11
- Adibekyan, V. Zh., Sousa, S. G., Santos, N. C., et al. 2012, *A&A*, 545, A32
- Allende Prieto, C., Lambert, D. L., & Asplund, M. 2001, *ApJ*, 556, L63
- Anstee, S. D., & O'Mara, B. J. 1995, *MNRAS*, 276, 859
- Asplund, M. 2005, *ARA&A*, 43, 481

- Asplund, M., Grevesse, N., Sauval, A. J., & Scott, P. 2009, *ARA&A*, 47, 481
- Barklem, P. S. & Asplund-Johansson, J. 2005, *A&A*, 435, 373
- Barklem, P. S., & O'Mara, B. J. 1998, *MNRAS*, 300, 863
- Barklem, P. S., Piskunov, N., & O'Mara, B. J. 2000, *A&AS*, 142, 467
- Baumüller, D., & Gehren, T. 1996, *A&A*, 307, 961
- Bedell, M., Meléndez, J., Bean, J. L., et al. 2014, *Ap*, 795, 23
- Bensby, T., Feltzing, S., & Oey, M. S. 2014, *A&A*, 562, A71
- Bensby, T., Zenn, A. R., Oey, M. S., & Feltzing 2007, *ApJ*, 663, L13
- Bergemann, M. 2011, *MNRAS*, 413, 2184
- Bergemann, M., & Cescutti, G., 2010, *A&A*, 522, A9
- Bond, J. C., O'Brien, D. P., & Lauretta, D. S. 2010, *ApJ*, 715, 1050
- Butler, R. P., Wright, J. T., Marcy, G. W., et al. 2006, *ApJ*, 646, 505
- Caffau, E., Ludwig, H.-G., Steffen, M., Freytag, B., & Bonifacio, P. 2011, *Solar Phys.*, 268, 255
- Casagrande, L., Ramírez, I., Meléndez, J., Bessell, M., & Asplund, M. 2010, *A&A*, 512, A54
- Christensen-Dalsgaard, J., Däppen, W., Ajukov, S. V., et al. 1996 *Science*, 272, 1286
- Conroy, C., Graves, G. J., & van Dokkum, P. G. 2014, *ApJ*, 780, 33
- Damasso, M., Biazzo, K., Bonomo, A. S., et al. 2015, *A&A*, 575, A111
- Delgado Mena, E., Israelian, G., González Hernández, J. I., et al. 2010, *ApJ*, 725, 2349
- Edvardsson, B., Andersen, J., Gustafsson, B., et al. 1993, *A&A*, 275, 101
- Epstein, C. R., Johnson, J. A., Dong, S., et al. 2010, *ApJ*, 709, 447
- Fabbian, D., Khomenko, E., Moreno-Insertis, F., & Nordlund, Å. 2010, *ApJ*, 724, 1536
- Fabbian, D., & Moreno-Insertis, F. 2015, *ApJ*, 802, 96
- Fabbian, D., Moreno-Insertis, F., Khomenko, E., & Nordlund, Å. 2012, *A&A*, 548, A35
- Fortney, J. J. 2012, *ApJ*, 747, L27
- Gaidos, E. 2015, *ApJ*, in press (arXiv:1502.0699)
- Gonzalez, G., Carlson, M. K., & Tobin, R. W. 2010, *MNRAS*, 407, 314
- González Hernández, J. I., Delgado-Mena, E., Sousa, S. G., et al. 2013, *A&A*, 552, A6
- González Hernández, J. I., Israelian, G., Santos, N. C., et al. 2010, *ApJ*, 720, 1592
- Gustafsson, B., Edvardsson, B., Eriksson, K., et al. 2008, *A&A*, 486, 951
- Haywood, M., Di Matteo, P., Lehnert, M. D., Katz, D., & Gómez, A. 2013, *A&A* 560, A109
- Haywood, M., Di Matteo, P., Snaith, O., & Lehnert, M. D. 2015, *A&A*, in press (arXiv:1504.02019)
- Johansson, S., Litzén, U., Lundberg, H., & Zhang, Z. 2003, *ApJ*, 584, L107
- Jones, H. R. A., Butler, R. P., Tinney, C. G., et al. 2006, *MNRAS*, 369, 249
- Karakas, A. I. 2010, *MNRAS*, 403, 1413
- Kim, Y.-C., Demarque, P., Yi, S. K., & Alexander, D. R. 2002, *ApJS*, 143, 499
- Kiselman, D. 1993, *A&A*, 275, 269
- Kobayashi, C., Umeda, H., Nomoto, K., Tominaga, N., & Ohkubo, T. 2006, *ApJ*, 653, 1145
- Kurucz, R. 1993, *ATLAS9 Stellar Atmosphere Programs and 2 km s⁻¹ grid*. Kurucz CD-ROM No. 13. Cambridge, Mass.: Smithsonian Astrophysical Observatory, 1993, 13
- Lemasle, B., de Boer, T. J. L., Hill, V., et al. 2014, *A&A*, 572, A88
- Letarte, B., Hill, V., Tolstoy, E., et al. 2010, *A&A*, 523, A17
- Lind, K., Asplund, M., Barklem, P. S., & Belyaev, A. K. 2011, *A&A*, 528, A103
- Lind, K., Bergemann, M., & Asplund, M. 2012, *MNRAS*, 427, 50
- Liu, F., Asplund, M., Ramírez, I., Yong, D., & Meléndez, J. 2014, *MNRAS*, 442, L51
- Lodders, K. 2003, *ApJ*, 591, 1220
- Maldonado, J., Eiroa, C., Villaver, E., Montesinos, B., & Mora, A. 2015, *A&A*, in press (arXiv:1502.07100)
- Mashonkina, L., Korn, A. J., & Przybilla, N. 2007, *A&A*, 461, 261
- Mayor, M., Marmier, M., Lovis, C., et al. 2011, (arXiv:1109.2497)
- Mayor, M., Pepe, F., Queloz, D., et al. 2003, *The Messenger*, 114, 20
- Meléndez, J., Asplund, M., Gustafsson, B., & Yong, D. 2009, *ApJ*, 704, L66
- Meléndez, J., Bergemann, M., Cohen, J. G., et al. 2012, *A&A*, 543, A29
- Meléndez, J., Ramírez, I., Karakas, A. I., et al. 2014a, *ApJ*, 791, 14
- Meléndez, J., Schirbel, L., Monroe, T. W. R., et al. 2014b, *A&A*, 567, L3
- Monroe, T. W. R., Meléndez, J., Ramírez, I., et al. 2013, *ApJ*, 774, L32
- Moore, C. S., Uitenbroek, H., Rempel, M., Criscuoli, S., & Rast, M. P. 2015, *ApJ*, 799, 150
- Mulchay, J. S., Kasliwal, M. M., & Kollmeier, J. A. 2014, *ApJ*, 780, L34
- Neves, V., Santos, N. C., Sousa, S. G., Correia, A. C. M., & Israelian, G. 2009, *A&A*, 497, 563
- Nissen, P. E. 2013, *A&A*, 552, A73
- Nissen, P. E., Chen, Y. Q., Carigi, L., Schuster, W. J., & Zhao, G. 2014, *A&A*, 568, A25
- Nissen, P. E., Primas, F., Asplund, M., & Lambert, D. L. 2002, *A&A*, 390, 235
- Nissen, P. E., & Schuster, W. J. 1997, *A&A*, 326, 751
- Nissen, P. E., & Schuster, W. J. 2010, *A&A*, 511, L10
- Nissen, P. E., & Schuster, W. J. 2011, *A&A*, 530, A15
- Nissen, P. E., & Schuster, W. J. 2012, *A&A*, 543, A28
- Olsen, E. H. 1983, *A&AS*, 54, 55
- Önehag, A., Gustafsson, B., & Korn, A. 2014, *A&A*, 562, A102
- Perets, H. B., Gal-Yam, A., & Mazzali, P. A. 2010, *Nature*, 465, 322
- Petigura, E. A., & Marcy, G. W. 2011, *ApJ*, 735, 41
- Ramírez, I., Meléndez, J., & Asplund, M. 2009, *A&A*, 508, L17
- Ramírez, I., Meléndez, J., & Asplund, M. 2014a, *A&A*, 561, A7
- Ramírez, I., Meléndez, J., & Bean, J., et al. 2014b, *A&A*, 572, A48
- Ramírez, I., Meléndez, J., Cornejo, D., Roederer, I. U., & Fish, J. R. 2011, *ApJ*, 740, 76
- Schuler, S. C., Flateau, D., Cunha, K., et al. 2011, *ApJ*, 732, 55
- Scott, P., Asplund, M., Grevesse, N., Bergemann, M., & Sauval, A. J. 2015a, *A&A*, 573, A26
- Scott, P., Asplund, M., Grevesse, N., & Sauval, J. 2009, *ApJ*, 691, L119
- Scott, P., Grevesse, N., Asplund, M., et al. 2015a, *A&A*, 573, A25
- Shi, J. R., Gehren, T., Butler, K., Mashonkina, L. I., & Zhao, G. 2008, *A&A*, 486, 303
- Sousa, S. G., Santos, N. C., Mayor, M., et al. 2008, *A&A*, 487, 373
- Takeda, Y., Hashimoto, O., Taguchi, H., et al. 2005, *PASJ*, 57, 751
- Takeda, Y., & Honda, S. 2005, *PASJ*, 57, 65
- Teske, J. K., Ghezzi, L., Cunha, K., et al. 2015, *ApJ*, 801, L10
- Teske, J. K., Cunha, K., Smith, V. V., Schuler, S. C., & Griffith, C. A. 2014, *ApJ*, 788, 39
- Travaglio, C., Gallino, R., Arnone, E., et al. 2004, *ApJ*, 601, 864
- Trujillo Bueno, J., Shchukina, N., & Asensio Ramos, A. 2004, *Nature*, 430, 326
- Tucci Maia, M., Meléndez, J., & Ramírez, I. 2014, *ApJ*, 790, L25
- Turcotte, S., & Wimmer-Schweingruber, R. F. 2002, *J. Geophys. Res.*, 107(A12), 1442
- Unsöld, A. 1955, *Physik der Sternatmosphären*, 2nd ed. (Berlin: Springer Verlag)
- van Leeuwen, F. 2007, *Hipparcos, the New Reduction of the Raw Data*, (Astrophys. Space Sci. Library, vol. 350; Dordrecht, Springer)
- Venn, K. A., Irwin, M., Shetrone, M. D., et al. 2004, *AJ*, 128, 1177
- Yi, S., Demarque, P., Kim, Y. -C., et al. 2001, *ApJS*, 136, 417
- Yi, S. K., Kim, Y. -C., & Demarque, P. 2003, *ApJS*, 144, 259
- Zhao, G., & Gehren, T. 2000, *A&A*, 362, 1077

Table 2. List of spectral lines.

Element	Wavelength [Å]	Exc. pot. [eV]	EW _⊙ [mÅ]
C I	5052.15	7.685	36.0
C I	5380.32	7.685	21.4
[O I]	6300.31	0.000	3.6
Na I	6154.23	2.102	38.2
Na I	6160.75	2.104	58.8
Mg I	4730.04	4.340	71.5
Mg I	5711.10	4.345	105.6
Al I	6696.03	3.143	37.7
Al I	6698.67	3.143	21.0
Si I	5517.55	5.080	13.8
Si I	5645.62	4.929	36.6
Si I	5665.56	4.920	41.2
Si I	5793.08	4.929	43.9
Si I	6125.03	5.614	32.5
Si I	6145.02	5.616	38.8
Si I	6243.82	5.616	48.1
Si I	6244.48	5.616	46.3
Si I	6721.84	5.862	44.7
Si I	6741.63	5.984	15.9
S I	6045.98	7.868	18.3
S I	6052.67	7.870	11.8
S I	6743.58	7.866	8.6
S I	6757.14	7.870	18.7
Ca I	5260.39	2.521	32.8
Ca I	5512.99	2.933	88.3
Ca I	5581.98	2.523	96.5
Ca I	5590.13	2.521	92.6
Ca I	5867.57	2.933	25.0
Ca I	6166.44	2.521	71.1
Ca I	6455.60	2.523	57.4
Ti I	4913.62	1.873	51.5
Ti I	5113.45	1.443	27.9
Ti I	5219.71	0.021	28.1
Ti I	5295.78	1.067	12.7
Ti I	5490.16	1.460	22.2
Ti I	5739.48	2.249	8.0
Ti I	5866.46	1.066	48.6
Ti I	6091.18	2.267	15.2
Ti I	6126.22	1.066	22.6
Ti I	6258.11	1.443	52.2
Ti I	6261.11	1.429	48.5
Ti II	5211.54	2.590	33.7
Ti II	5381.03	1.565	60.9
Ti II	5418.77	1.582	49.0
Cr I	5214.13	3.369	17.0
Cr I	5238.97	2.709	16.9
Cr I	5247.57	0.960	83.4
Cr I	5272.00	3.449	23.8
Cr I	5287.18	3.438	11.3
Cr I	5296.70	0.983	93.9
Cr I	5348.33	1.004	100.2
Cr I	5783.07	3.323	31.4
Cr I	5783.87	3.322	44.6
Cr I	6661.08	4.193	13.0
Cr II	5237.33	4.073	53.5
Cr II	5246.78	3.714	16.2
Fe I	5295.32	4.415	29.9
Fe I	5373.71	4.473	63.9
Fe I	5379.58	3.694	61.9

Table 2. continued

Element	Wavelength (Å)	Exc. pot. (eV)	EW_{\odot} (mÅ)
Fe I	5386.34	4.154	33.1
Fe I	5466.99	3.573	35.9
Fe I	5522.45	4.209	44.2
Fe I	5546.51	4.371	52.9
Fe I	5560.22	4.434	52.6
Fe I	5577.03	5.033	11.6
Fe I	5618.64	4.209	50.4
Fe I	5636.71	3.640	19.6
Fe I	5650.00	5.100	36.5
Fe I	5651.48	4.473	19.0
Fe I	5661.35	4.284	23.0
Fe I	5679.03	4.652	60.4
Fe I	5705.47	4.301	38.4
Fe I	5855.09	4.608	22.7
Fe I	6079.02	4.652	46.5
Fe I	6082.72	2.223	35.4
Fe I	6093.65	4.607	31.1
Fe I	6096.67	3.984	37.8
Fe I	6151.62	2.176	50.1
Fe I	6157.73	4.076	62.4
Fe I	6165.36	4.143	45.0
Fe I	6173.34	2.223	68.7
Fe I	6188.00	3.943	48.4
Fe I	6226.74	3.883	29.6
Fe I	6240.65	2.223	49.0
Fe I	6270.23	2.858	52.2
Fe I	6271.28	3.332	24.4
Fe I	6380.75	4.186	52.7
Fe I	6392.54	2.279	17.6
Fe I	6498.94	0.958	47.1
Fe I	6597.57	4.795	44.0
Fe I	6625.04	1.011	15.6
Fe I	6703.58	2.759	37.3
Fe I	6705.10	4.607	47.6
Fe I	6710.32	1.485	16.0
Fe I	6713.75	4.795	21.3
Fe I	6725.36	4.103	17.8
Fe I	6726.67	4.607	47.3
Fe I	6733.15	4.638	26.9
Fe I	6739.52	1.557	12.0
Fe I	6793.27	4.076	13.0
Fe I	6806.86	2.727	34.9
Fe I	6810.27	4.607	50.1
Fe I	6843.65	4.548	61.5
Fe II	5414.08	3.222	27.3
Fe II	5425.26	3.200	41.5
Fe II	6084.10	3.200	21.2
Fe II	6149.25	3.889	36.7
Fe II	6247.56	3.892	53.1
Fe II	6369.46	2.891	18.8
Fe II	6416.93	3.892	40.1
Fe II	6432.68	2.892	41.6
Fe II	6456.39	3.904	63.4
Ni I	4953.21	3.740	56.2
Ni I	5010.94	3.635	49.9
Ni I	5643.09	4.164	15.9
Ni I	5805.23	4.167	41.5
Ni I	6086.29	4.266	44.2
Ni I	6108.12	1.676	65.6

Table 2. continued

Element	Wavelength (Å)	Exc. pot. (eV)	EW_{\odot} (mÅ)
Ni I	6130.14	4.266	22.3
Ni I	6176.82	4.088	64.1
Ni I	6177.25	1.826	14.8
Ni I	6204.61	4.088	22.1
Ni I	6378.26	4.154	32.8
Ni I	6643.64	1.676	94.7
Ni I	6767.78	1.826	79.7
Ni I	6772.32	3.657	50.1
Zn I	4722.16	4.030	71.6
Zn I	4810.54	4.080	75.0
Zn I	6362.35	5.790	20.4
Y II	4883.69	1.084	59.5
Y II	5087.43	1.084	48.7
Y II	5200.42	0.992	38.1

Table 3. Atmospheric parameters and abundance ratios.

Star	T_{eff} K	$\log g$	[Fe/H]	ξ_{turb} km s ⁻¹	[C/Fe]	[O/Fe]	[Na/Fe]	[Mg/Fe]	[Al/Fe]	[Si/Fe]	[S/Fe]	[Ca/Fe]	[Ti/Fe]	[Cr/Fe]	[Ni/Fe]	[Zn/Fe]	[Y/Fe]
HD2071	5724	4.490	-0.084	0.96	-0.022	-0.022	-0.032	0.001	-0.002	0.001	-0.007	0.024	0.019	0.005	-0.029	-0.026	0.040
HD8406	5730	4.479	-0.105	0.95	-0.036	-0.028	-0.059	0.000	-0.020	-0.010	-0.021	0.031	0.009	0.010	-0.041	-0.044	0.050
HD20782	5776	4.345	-0.058	1.04	-0.019	0.024	-0.086	0.011	0.015	-0.006	-0.013	0.015	0.028	-0.004	-0.042	-0.019	-0.110
HD27063	5779	4.469	0.064	0.99	-0.082	-0.078	-0.041	-0.018	-0.029	-0.019	-0.039	0.023	-0.005	0.016	-0.022	-0.055	0.067
HD28471	5754	4.380	-0.054	1.02	-0.023	0.006	-0.013	0.037	0.065	0.022	-0.010	0.026	0.046	-0.007	-0.005	0.018	-0.067
HD38277	5860	4.270	-0.070	1.17	-0.012	0.049	-0.078	0.012	0.012	0.006	-0.017	0.007	0.023	-0.018	-0.042	-0.016	-0.129
HD45184	5871	4.445	0.047	1.06	-0.069	-0.055	-0.031	-0.009	-0.015	-0.005	-0.045	0.015	0.011	-0.002	-0.020	-0.030	0.040
HD45289*	5718	4.284	-0.020	1.06	0.058	0.146	-0.009	0.100	0.128	0.055	0.056	0.049	0.100	0.002	0.006	0.096	-0.094
HD71334	5701	4.374	-0.075	0.98	-0.024	0.031	-0.034	0.039	0.063	0.019	-0.003	0.034	0.041	0.000	-0.014	-0.007	-0.076
HD78429	5756	4.272	0.078	1.05	-0.025	0.004	-0.055	0.022	0.034	-0.002	0.001	0.006	0.019	0.005	-0.020	0.014	-0.101
HD88084	5768	4.424	-0.091	1.02	0.017	-0.010	0.003	0.028	0.053	0.021	0.008	0.019	0.035	-0.009	-0.003	0.009	-0.044
HD92719	5813	4.488	-0.112	1.00	-0.060	-0.009	-0.050	0.002	-0.014	0.003	-0.062	0.031	0.021	-0.001	-0.044	-0.046	0.042
HD96116	5846	4.503	0.006	1.02	-0.088	-0.046	-0.100	-0.041	-0.063	-0.036	-0.052	0.019	-0.019	0.013	-0.056	-0.085	0.095
HD96423	5714	4.359	0.113	0.99	-0.056	-0.076	0.008	0.021	0.056	0.005	-0.035	0.005	0.028	0.005	0.021	-0.014	-0.033
HD134664	5853	4.452	0.093	1.01	-0.116	-0.087	-0.058	-0.022	-0.035	-0.019	-0.048	0.009	0.004	0.006	-0.022	-0.055	0.050
HD146233	5809	4.434	0.046	1.02	-0.066	-0.028	-0.028	-0.010	-0.020	-0.007	-0.029	0.010	0.009	0.010	-0.013	-0.036	0.041
HD183658	5809	4.402	0.035	1.04	-0.002	-0.040	0.024	0.009	0.018	0.009	0.006	0.002	0.008	-0.005	0.013	0.008	-0.025
HD208704	5828	4.346	-0.091	1.08	-0.009	0.033	-0.062	0.017	0.023	0.005	-0.020	0.015	0.024	-0.012	-0.033	0.000	-0.111
HD210918*	5748	4.319	-0.095	1.07	0.054	0.146	-0.057	0.072	0.102	0.029	0.032	0.043	0.080	-0.012	-0.029	0.034	-0.077
HD220507*	5690	4.247	0.013	1.07	0.102	0.159	0.036	0.126	0.153	0.071	0.084	0.051	0.114	0.004	0.017	0.121	-0.085
HD222582	5784	4.361	-0.004	1.07	-0.001	0.043	0.014	0.037	0.058	0.028	-0.021	0.015	0.041	0.000	0.005	0.025	-0.065

Notes. (*) α -enhanced star.